AEDC-TR-66-37

MASS TRANSFER AND FIRST-ORDER BOUNDARY-LAYER EFFECTS ON SHARP CONE DRAG

Clark H. Lewis, Ernest O. Marchand, and Herbert R. Little

ARO, Inc.

March 1966

VON KÁRMÁN GAS DYNAMICS FACILITY
ARNOLD ENGINEERING DEVELOPMENT CENTER
AIR FORCE SYSTEMS COMMAND
ARNOLD AIR FORCE STATION, TENNESSEE

NOTICES

When U. S. Government drawings specifications, or other data are used for any purpose other than a definitely related Government procurement operation, the Government thereby incurs no responsibility nor any obligation whatsoever, and the fact that the Government may have formulated, furnished, or in any way supplied the said drawings, specifications, or other data, is not to be regarded by implication or otherwise, or in any manner licensing the holder or any other person or corporation, or conveying any rights or permission to manufacture, use, or sell any patented invention that may in any way be related thereto.

Qualified users may obtain copies of this report from the Defense Documentation Center.

References to named commercial products in this report are not to be considered in any sense as an endorsement of the product by the United States Air Force or the Government.

MASS TRANSFER AND FIRST-ORDER BOUNDARY-LAYER EFFECTS ON SHARP CONE DRAG

Clark H. Lewis, Ernest O. Marchand, and Herbert R. Little
ARO, Inc.

FOREWORD

The work reported herein was done at the request of Headquarters, Arnold Engineering Development Center (AEDC), Air Force Systems Command (AFSC), under Program Element 62405334, Project 8953, Task 895303.

The results presented were obtained by ARO, Inc. (a subsidiary of Sverdrup and Parcel, Inc.), contract operator of the AEDC, AFSC, Arnold Air Force Station, Tennessee, under Contract AF40(600)-1200. The research was conducted under ARO Project No. VW3507, and the manuscript was submitted for publication on January 27, 1966.

The information contained in this report was presented as a paper at the AIAA 3rd Aerospace Sciences Meeting in New York, N. Y., January 24-26, 1966.

The authors are pleased to acknowledge the assistance of C. C. Limbaugh, E. G. Burgess, III, and M. Brown, Jr., ARO, Inc., in making the numerical calculations. The assistance of J. L. Potter and D. E. Boylan, ARO, Inc., in obtaining the experimental AEDC-von Kármán Gas Dynamics Facility (VKF) low density tunnel data is also acknowledged.

This technical report has been reviewed and is approved.

Larry R. Walter
1st Lieutenant, USAF
Gas Dynamics Division
DCS/Research

Donald R. Eastman, Jr.
DCS/Research

ABSTRACT

A theoretical model is developed based on an iterated perfect gas inviscid-viscous flow field which includes first-order displacement (viscous interaction), transverse curvature, wall slip, and temperature jump in addition to mass transfer effects. The effects of inviscid (tangent cone) and viscous (nonsimilar laminar boundary layer) flow field matching conditions are also considered. Numerical results are compared with experimental and analytical results of King and Talbot (AIAA J., 1964) for a 5-deg half-angle cone at M_∞ = 3.93 and 5.64. The predicted viscous-induced pressure without mass transfer and the zero-lift drag with and without injection were in agreement with the experimental data within experimental uncertainty. The theoretical model was also used to predict zero-lift drag of a 9-deg half-angle cone at M_∞ = 9.37 and 10 and Re_∞/in. = 400 to 45,000 for a range of wall-to-stagnation temperature ratios. Again, in general, without mass transfer the predictions were within experimental uncertainty. The inability of the theoretical model to adequately treat nonuniform mass transfer distributions is discussed. At the lowest Reynolds number the effects of slip were most significant. At all conditions the effects of inviscid-viscous flow field matching were significant. Experimental zero injection equilibrium wall temperature distributions and cool-wall pressure data are given at M_∞ ~ 10 and Re_∞/in. = 400 to 2600.

CONTENTS

ILLUSTRATIONS

TABLES

TABLES (Continued)

NOMENCLATURE

A_B	Base area
A_w	Surface area
C_{D_f}	Skin-friction drag coefficient referenced to base area
C_{D_p}	Pressure drag coefficient
C_f	Local skin-friction coefficient, $2\tau_w/\rho u^2$
C_∞	Constant of proportionality in linear viscosity law, $(T_\infty/T_w)(\mu_w/\mu_\infty)$
f'	Velocity ratio, u/u_e
g	Stagnation enthalpy ratio, H/H_e
H	Stagnation enthalpy
h	Static enthalpy
h_{ref}	Reference enthalpy (2.119×10^8 ft^2/sec^2)
L	Slant cone length
ℓ	Axial length
M	Mach number
$\dot{m}$	Mass transfer rate
Pr	Prandtl number
p	Static pressure
p_o'	Normal shock stagnation (pitot) pressure
q	Heat-transfer rate
R	Gas constant

Re	Reynolds number
r	Radius normal to axis of symmetry
r_B	Base radius
r_{eff}	Effective wall radius, $r_w(x) + \cos \theta_c \, \delta^{*(n-1)}$
St	Stanton number, $q/\rho u \, (H_o - H_w)$
T	Temperature, °K
t	Wall thickness
u	Tangential velocity component
v	Normal velocity component
$\bar{v}_\infty$	Hypersonic viscous parameter, $M_\infty \, (C_\infty/Re_{\infty,\ell})^{1/2}$
x	Surface distance measured from cone tip
x_i	Origin of continuum boundary layer plus slip and temperature jump
y	Distance normal to the surface
z	Axial distance measured from cone tip
γ	Ratio of specific heats
δ	Boundary-layer thickness (where $u/u_e = 0.995$)
δ^*	Boundary-layer displacement thickness
η	Transformed coordinate normal to the wall, $(u_e L/\rho_* \mu_* x)^{1/2} \int \rho \, dy$
θ_c	Cone half-angle
λ	Mean free path
μ	Viscosity
ρ	Mass density
τ	Shear stress

SUBSCRIPTS

c	Corrected pressure
e	Local inviscid conditions at the "edge" of the boundary layer
i	Initial location of continuum boundary layer with slip
inv	Inviscid conditions without wall boundary layer

m	Measured pressure
o	Free-stream stagnation conditions
w	Wall conditions
∞	Free-stream conditions
$*$	Reference conditions at inviscid sharp cone conditions

SUPERSCRIPTS

(n)	Iteration index corresponding to the pressure distribution over the "effective" body $r_{eff}^{(n)} = r_w + \cos \theta_c \, \delta^{*(n-1)}$. Zero denotes the inviscid sharp cone edge conditions. Iteration with slip is denoted $(ns + js)$ where n is no-slip and j is slip iteration number.
	Differentiation with respect to the transformed variable η

SECTION I
INTRODUCTION

For several years viscous effects on sharp and blunt slender cones have been studied in the Arnold Engineering Development Center, von Kármán Gas Dynamics Facility (Refs. 1-3). The large viscous-induced drag increment at zero-lift observed in these studies encouraged Whitfield and Griffith (Ref. 2) to consider the effects of mass transfer to reduce the drag. They experimentally investigated the effects of tangential injection of gases on zero-lift drag at M_∞ = 10 and 21. The experimental investigations have recently been extended by Little and Griffith (Ref. 4) to include the effects of normal injection on zero-lift drag at $M_\infty \cong 10$. The present report presents an analysis of some of the latter experimental results after developing a theoretical model and making comparisons with some experimental and theoretical data at supersonic conditions.

King and Talbot (Refs. 5 and 6) studied the effects of normal gas injection on the pressure distributions and zero-lift drag of a sharp 5-deg half-angle cone in the Berkeley Low Density Wind Tunnel. Experimental data were taken at near adiabatic wall conditions ($T_w/T_o \simeq 0.96$) and Re_∞/in. = 1765 and 6286 at M_∞ = 3.93 and 5.64, respectively. They gave an analysis based on approximate methods which is described in more detail below. The experimental and theoretical data of King and Talbot are compared with the results from methods developed in the present report.

King and Talbot (Ref. 6) and Little and Griffith (Ref. 4) obtained experimental data for binary boundary layers with injected gases other than the test gases (air and nitrogen) used in the wind tunnel experiments. For example, the latter investigators also used helium, argon, and carbon dioxide as injected gases. In the present report, however, only the cases of injection of air into air or nitrogen into air or nitrogen will be considered.

The experimental drag data of Little and Griffith were taken with a partially porous 9-deg half-angle cone at M_∞ = 9.37 and 10 and for a span of Reynolds numbers Re_∞/in. = 388 to 42,640. The estimated range of wall-to-stagnation temperature ratios was from 0.2 to 0.75. Quite recently some experimental data were obtained on the equilibrium wall temperature variation over a hollow cone in the AEDC-VKF low density tunnel (Gas Dynamic Wind Tunnel, Hypersonic (L)), and the pressure was measured on a sharp, water-cooled cone at Re_∞/in. = 388, 1602, and 2606 in the same wind tunnel. These recent experimental data are also included in this report.

Under certain experimental conditions the effects of slip and temperature jump were significant, and the present analysis presents an approximate treatment of those effects on pressure and heat-transfer distributions and zero-lift drag. The effects of slip were considered significant upon comparison of the experimental results with the numerical results of the present investigation when slip and temperature jump effects were neglected.

Before further considering the theoretical model used in the present report, the experimental conditions which were studied will be presented.

SECTION II
EXPERIMENTAL CONDITIONS STUDIED

2.1 WIND TUNNELS

The experimental data used in the present study were obtained at Berkeley by King and Talbot (Refs. 5 and 6) and at the AEDC-VKF by Little and Griffith (Ref. 4). Some details concerning their experimental investigations are given in this section for the convenience of the reader.

Three wind tunnels were used in the experimental studies: viz. the low density wind tunnel at Berkeley and two AEDC-VKF Mach 10 tunnels (Gas Dynamic Wind Tunnels, Hypersonic (C) and (L)). The Berkeley tunnel is an unheated air, continuous flow, free jet facility using axisymmetric contoured nozzles to produce Mach numbers of 3.93 and 5.64. Tunnel C is a continuous flow, hypersonic wind tunnel. Air, heated to a temperature sufficient to avoid liquefaction, expands through a contoured, axisymmetric nozzle to the 50-in.-diameter test section. The free-stream Reynolds number was varied by changing the free-stream stagnation (reservoir) pressure. Tunnel L is an arc-heated, continuous flow facility using interchangeable axisymmetric contoured nozzles to produce nominal Mach 10 flow. Nitrogen was used as the test gas.

The flow conditions from the experimental investigations which are considered in the present report are given in Table I. The experimental conditions are given in the first row, and the data used in the numerical calculations are given in the second row. For most cases the perfect gas data for the numerical calculations were based on the measured free-stream pitot pressure and (equilibrium) free-stream stagnation temperature. The equilibrium stagnation enthalpy was then determined, and the ideal gas (γ = 1.4) stagnation temperature was computed. Ideal gas, normal shock, and one-dimensional, isentropic flow

relations were then used to obtain the free-stream and reservoir conditions. This procedure gave an ideal gas stagnation temperature somewhat higher than the corresponding equilibrium value, and this also produced other differences as shown in Table I.

2.2 MODELS

The force models used for the experimental studies were sharp cones with partially porous surfaces. King's models were 5-deg half-angle cones with small solid base and tip regions (Fig. 1a). The porous material was sintered, powdered, Monel® metal particles. An experimentally determined mass flux distribution is shown in Fig. 2. King states that the distribution of mass flux represents a circumferential average and should be regarded as qualitative rather than quantitative. Surface pressure data were taken with mass injection, but since the porous surface near the taps was distorted the pressure data were affected. Therefore, the only experimental pressure data of King and Talbot used in the present report were taken on solid (no injection) cone models.

The AEDC-VKF force model was a sharp, 9-deg half-angle cone with a base diameter of 0.75-in. (Fig. 1b). The solid nose was followed by a porous afterbody machined from General Electric 50-percent dense nickel Foametal®. The impervious nose extended over 0.57 of the (slant) length of the cone. Over the remainder of the cone, however, the constant density and thickness of the wall gave a mass flux distribution constant within ±15 percent as obtained from a hot-wire anemometer survey. Figure 2 also shows a typical mass flux distribution for the AEDC-VKF model.

The zero injection drag data were taken after the model had been in the flow a sufficient time to reach approximately 90 percent of the equilibrium wall temperature (as indicated from changes in measured drag data). Although no experimental wall temperature data exist for the force model, the values quoted below for a hollow stainless steel model are believed representative for the zero-injection drag data as well.

The pressure was measured at two locations on a water-cooled copper model (Fig. 1c) in Tunnel L. The thin copper wall was cooled to the water temperature (~ 293°K), and the temperature was assumed to remain constant over the entire surface.

The wall temperature was measured with a thin-wall ($t \leq 0.010$ in.) stainless steel model as shown in Fig. 1d. The output of thermocouples

welded to the inside surface of the model was recorded as a function of time. Wall temperatures reached 90 percent of the equilibrium value within one to three minutes, and equilibrium was reached within about ten minutes.

2.3 EXPERIMENTAL DATA AND PRECISION

The primary test measurements were axial force and surface pressures in the Berkeley experiments and axial force with and without mass transfer, and surface pressures and wall temperatures without mass transfer in the AEDC-VKF experiments. The estimated precision of these data is shown in the table below:

Source	Force, percent	Pressure, percent $\dot{m} = 0$	Pressure, percent $\dot{m} > 0$
Berkeley	±5	±2	±5
Tunnel C	±7	--	--
Tunnel L	±7	--	--

The experimental value of C_D for each value of injected mass flow used in the numerical calculations is shown in Table II, the experimental pressure data are shown in Table III, and wall temperature data are shown in Table IV. It should be noted that the drag data presented do not necessarily correspond to actual data points but rather were taken from fairings of the data.

Wall-to-stagnation temperatures are also tabulated. For the Berkeley tests the data were from readings of thermocouples located at the base of the model. The ratios for the AEDC-VKF zero injection data in Tunnel L are shown in Fig. 3, and the data from Tunnel C are from the previous data of Whitfield and Griffith. The accuracy of the thermocouple output is about ±2 percent; however no attempt has been made to assess effects of conduction losses through the wall. With injection the assumption is made that the cooled wall was maintained at the injection gas temperature (300°K).

No precision is quoted here for the pressure data in Tunnel L. However, the repeatability of the measured pressures was ±2 percent. (Also, the free-stream pitot pressure for the conditions $M_\infty = 9.37$ and $Re_\infty/in. = 1602$ was repeated and found to agree with previous tunnel calibrations within 1 percent.) Relatively large corrections to the measured pressure data are required to account for orifice size and heat-transfer effects,

and these effects will be discussed below. Because of the necessary corrections, a precision for the pressure data was more difficult to determine.

SECTION III
SOME THEORETICAL CONSIDERATIONS

3.1 KING AND TALBOT'S ANALYSIS

The Berkeley experimental data were analyzed by King and Talbot using (1) the similar boundary-layer solutions of Low (Ref. 7), (2) the effects of transverse curvature reported by Yasuhara (Ref. 8), (3) the inviscid flow field from the approximate tangent cone theory, and (4) the matching of the inviscid-viscous flow fields based on $d\delta^*/dx$. The "second-order" boundary-layer effects were assumed to be uncoupled, and a linear combination of these effects was added to the effects of mass transfer from Low's solutions.* Also, the effects of the impermeable nose were neglected in their calculations.

At the time the analysis was made by King and Talbot (1962), the above-mentioned theories and procedures were perhaps the best in existence. However, since that time certain theoretical developments have occurred which make a re-examination of their experimental data and comparisons with their analytical results of interest. This seems especially significant since their experimental data were taken at supersonic Mach numbers and moderate Reynolds number where other second-order boundary-layer effects (viz., external vorticity, slip, and temperature jump) should be small. Therefore, both their experimental data and analysis provide interesting data to test new theoretical models designed for application at hypersonic, cold-wall, low Reynolds number conditions.

3.2 PRESENT ANALYSIS

The basic theoretical model used in the numerical calculations was an iterated perfect gas (γ = 1.4) inviscid-viscous flow field. The viscous flow field was computed with the nonsimilar, laminar boundary-layer theory of Clutter and Smith (Ref. 9) which includes approximate transverse curvature terms. In addition, all boundary-layer calculations

*Low's flat-plate similarity solutions were transformed with the Mangler factor $(3)^{1/2}$.

were based on Sutherland's viscosity law and Prandtl number (Pr) = 0.71= constant. The inviscid flow field was computed from the approximate tangent-cone theory. The matching of the inviscid and viscous flow fields was treated in two ways: (1) using the usual matching condition $\theta_{eff} = \theta_c + \tan^{-1}(d\delta^*/dx)$ and (2) $\theta_{eff} = \theta_c + \tan^{-1}(v_e/u_e)$, where v_e/u_e was computed from the formula proposed by Li and Gross (Ref. 10).* Some comments on the matching conditions are given in Appendix I.

The inviscid-viscous flow field was iterated until there was negligible change in $\delta^*(x)$ or $p_e(x)$. At high Reynolds numbers only two iterations or three boundary-layer calculations were required. At low Reynolds numbers and especially at high injection rates, five iterations or six boundary-layer calculations were required. Moreover, significant effect of matching conditions was noted on the number of iterations required (the number being less with v_e/u_e since with this matching condition the inviscid outer flow was displaced less from the geometric wall $\theta_c(x)$ = constant). The method used for iterating the flow fields is discussed in Appendix II.

It should be noted that King and Talbot used a graphical method for matching the inviscid outer flow (tangent cone) with the viscous, boundary-layer edge conditions (Low's similar solutions). The matching was done simultaneously step by step along the body rather than obtaining successive approximations to the entire "effective" body as was done in the present investigation.

Because of the difficulties associated with iterating the inviscid-viscous flow field, most calculations presented in this report were based on a uniform injection (constant blowing) rate rather than constant $f_w \sim 1/x^{1/2}$ as required for similarity (see, e.g., Low, Ref. 7). Uniform injection more nearly represented the actual mass flux distributions over the porous region of the model in the $M_\infty = 10$ experiments and appears to be a reasonable approximation for the experimental distributions of King and Talbot. The effects of the impermeable nose region were investigated for the King and Talbot conditions and for one set of conditions at $M_\infty = 10$.

The experimental data of King and Talbot indicated a near-constant, wall-to-stagnation temperature ratio $T_w/T_o = 0.96$. Most of the numerical calculations for the present report at $M_\infty \sim 10$ were completed before the experimental wall temperature data were available. The wall-to-stagnation temperature ratios assumed in the calculations are indicated

*Hereafter the matching conditions will be denoted as $d\delta^*/dx$ or v_e/u_e.

in the figures where comparisons with experimental data are given. In all calculations the wall temperature was assumed to be constant, and the effects of wall temperature distributions such as shown in Fig. 3 have not been investigated.

The effects of slip and temperature jump were investigated at all conditions. The boundary-layer theory of Clutter and Smith (Ref. 9) was modified to include these effects. For more direct comparison with others, the mean free path was evaluated at the wall temperature, T_w, rather than at the slip condition $T(\eta = 0)$; however, this is not a necessary condition for the numerical procedure. Details of the procedure used in the present investigation are given in Appendix III.

It should be noted that the so-called second-order boundary-layer effects have all been treated as first-order effects. The first-order momentum and energy equations included (approximate)* transverse curvature terms, and the boundary conditions were modified to include slip and temperature jump. Moreover, the displacement effect is considered a first-order effect since the inviscid and viscous flow fields were iterated to "convergence". This is not, however, internally consistent since the outer flow was treated as inviscid (see Van Dyke, Ref. 1), and low density effects on the shock wave (e.g., finite thickness, curvature, and slip) were neglected (see Pan and Probstein, Ref. 12). These deficiencies can, in principle, be eliminated by a proper treatment of the "outer" flow.

SECTION IV
RESULTS AND DISCUSSION

The theoretical model used in the present report was tested against King and Talbot's experimental data and analytical results at $M_\infty = 3.93$ and 5.64. The theoretical model was then used to analyze the AEDC-VKF experimental data of Little and Griffith at $M_\infty = 9.37$ and 10. A large volume of interesting results were generated; however, the data presented herein will be confined to some of the more significant results.

4.1 BERKELEY CONDITIONS

The inviscid-viscous flow field was iterated as described above and in Appendix II. For convenience of comparison with the analytical results

*See the revised version of Clutter and Smith (Ref. 9).

of King and Talbot at $M_\infty = 5.64$ and $Re_\infty/in. = 6200$, the ratio δ^*/r_w was computed without mass transfer and is shown in Fig. 4. Excellent agreement was found with King and Talbot's results using the $d\delta^*/dx$ matching condition and the similar solutions of Low. The matching condition v_e/u_e predicted a slightly larger δ^* since the inviscid outer flow was displaced less by the boundary layer, and thus the viscous-induced pressure was less which in turn produced larger boundary-layer and displacement thicknesses. Under these conditions, transverse curvature had a negligible effect on $\delta^*(x)$.

The viscous-induced pressure increment $(p - p_{inv})/p_{inv}$ at $M_\infty = 3.93$ and 5.64 is shown in Fig. 5. The effects of matching condition and transverse curvature (TVC) were also considered. Using the matching condition v_e/u_e gave results which were in better agreement with the experimental pressure data of King and Talbot, especially at $M_\infty = 5.64$. The effects of slip and temperature jump are also shown. As suggested by King (Ref. 5), the effects of slip and temperature jump on the pressure distribution were indeed small. However, we will see later that the effects on the zero-lift drag are somewhat larger.

The effects of uniform mass transfer on the viscous-induced pressure increment at $M_\infty = 5.64$ are shown in Fig. 6. At the highest injection rate considered (0.09375 lbm/hr), the effects of matching conditions are also shown. At high injection rates the effects of matching conditions on the viscous-induced pressure increment became more important especially over the forward portion of the cone as shown in Fig. 6.

The ratio of local skin-friction coefficients $C_f/C_f^{(0)}$ at $M_\infty = 5.64$ is shown in Fig. 7, where $C_f^{(0)}$ is the value without viscous interaction, transverse curvature, or mass transfer. The separate and combined effects of viscous interaction and transverse curvature at zero injection are in contrast with the King and Talbot results. As noted by King (Ref. 5), $C_f^{(n)}/C_f^{(0)}$ should be greater than unity; however, his analysis predicted $C_f^{(n)}/C_f^{(0)} < 1$, a result which he attributed to his neglecting the viscous-induced axial pressure gradient by using the flat-plate results of Low (Ref. 7). The effect of transverse curvature on C_f based on the approximate theory of Clutter and Smith was in substantial agreement with King and Talbot's prediction using the theory of Yasuhara. The coupled and uncoupled effects of viscous interaction and transverse curvature on C_f could be seen by comparing the results denoted $VI^{(2)} + TVC^{(0)}$ with $(VI + TVC)^{(2)}$. The comparison (not shown in Fig. 7) indicated excellent agreement. This tends to support the usual assumption of linear independence of these second-order effects. The results denoted $(VI + TVC)^{(2)}$, however, have treated both as coupled first-order effects.

Three injection laws, viz., (1) $\rho_w v_w$ · constant, (2) f_w = constant, and (3) $\rho_w v_w = \phi(x)$ from the experimentally measured distribution of King and Talbot at $M_\infty = 5.64$, and their effects on friction drag are shown in Fig. 8. The effects of viscous interaction and transverse curvature coupled with the effects of injection laws on C_{D_f} are also shown. One significant result for the conditions considered was that the effects of the impervious nose and various injection laws on the friction drag were negligible. It is also significant that the prediction including viscous interaction and transverse curvature was in good agreement with the faired experimental data of King and Talbot. The latter data were obtained by subtracting the integrated experimental pressure drag from the experimentally measured total drag with a correction for mass injection (cf., King, Ref. 5).

Figure 9 shows the drag components and total drag coefficient $C_D = C_{D_f} + C_{D_p}$ from the present investigation compared with the experimental data and analytical results of King and Talbot at $M_\infty = 3.93$ and 5.64. The effects of viscous interaction, transverse curvature, and matching conditions with mass transfer are shown in the figure. The present results are in substantially better agreement with the experimental data than were the predictions of King and Talbot. In fact, the present results iterated to convergence and based on v_e/u_e matching conditions and with or without injection predicted total drag in agreement with the experimental data at $M_\infty = 5.64$ within the experimental uncertainty. This encouraging result should be tempered with the observation that the present analysis cannot be extended to much higher injection rates. Without viscous interaction, "blow-off" occurred far forward on the body at $\dot{m} \sim 0.12$ lbm/hr, whereas King's experimental data extended to $\dot{m} = 0.32$ lbm/hr before injection caused the total drag to reach a minimum.

The effects of slip and temperature jump on the zero injection drag at $M_\infty = 3.93$ and 5.64 are shown in Fig. 9 (the procedure used is discussed in more detail below for $M_\infty = 10$ conditions). At both Mach numbers, the effects of slip and temperature jump were about 5 percent, and this should be contrasted with the almost negligible effect on the viscous-induced pressure increment (see Fig. 5). If the present theoretical model is appropriate with respect to slip and temperature jump, it appears once again that experimental and theoretical zero-lift drag studies might be a useful tool for investigating another second-order boundary-layer effect. Of course, much work remains to solve the leading edge problem as well as the kinetic theory problems, such as reflection and accommodation coefficients. Although the predicted effects of slip at the Berkeley conditions were approximately equal to experimental uncertainty, the effects may be large enough to permit experimental verification at similar conditions.

4.2 AEDC-VKF CONDITIONS

The theoretical model was applied to the experimental data of Little and Griffith at $M_\infty = 10$. The effects of iteration on the displacement thickness and corresponding viscous-induced pressure increment with mass transfer at $Re_\infty/in. = 396$ are shown in Fig. 10. With injection the displacement thickness was substantially increased, and this in turn produced a large variation in the viscous-induced pressure increment with iteration. It should be noted that the solution had not converged with five iterations; however, the converged solution was bounded by the fourth and fifth iterations.

Figure 11 shows the effects of different injection laws on the zeroth iteration values of δ and δ^*. The difficulty of iterating the inviscid-viscous flow field near the beginning of the injection region ($x = 0.57$ to 0.75) prevented us from considering further the experimental distribution. Substantial differences in δ and δ^* caused by the two distributions (experimental and constant mass transfer) are evident in the figure.

Figure 12 shows the effects of mass transfer on the displacement and total boundary-layer thicknesses at $Re_\infty/in. = 396$. The thicknesses were, of course, increased; however, the character of the thicknesses was not substantially changed at this moderately high injection rate.

4.3 EFFECTS OF SLIP AND TEMPERATURE JUMP

Before presenting the comparisons of the numerical results with the experimental data for the effects of mass transfer on the drag coefficient at $M_\infty = 9.37$ and 10, the effects of slip and temperature jump on the numerical results are considered.

Figure 13 shows the ratio of the wall slip velocity to free-stream velocity and temperature jump at $M_\infty = 10$ and the lowest Reynolds number for which experimental data were available. The effects of matching conditions are shown, and the effects of viscous interaction are implicit since the calculations with slip and temperature jump were started from the converged no-slip solutions (see Appendix III). The temperature jump at the wall especially deserves a few comments. Near $x = 0$ where the slip velocity is largest, the temperature jump is smallest - a surprising result. However, the temperature jump is dominated by the quantity $(\partial h/\partial \eta)_{\eta=0}$ (see Appendix III). From the energy equation, $\partial h/\partial \eta = H_e g' - u_e^2 f' f''$, where prime denotes differentiation with respect to η. Thus with slip there exist values of f', g' and f'' such that $\partial h/\partial \eta = 0$ or $h(\eta = 0) = h_w$. Also, the solution based on $d\delta^*/dx$

matching conditions reached a maximum temperature jump near $x = 0.7$ and began to decrease. Of course, the asymptotic limit $T(\eta = 0) = T_w$ must be reached as $x \to \infty$; however, for this low Reynolds number condition there were large slip and temperature jump effects over the entire cone.

The effects of slip* and temperature jump on δ^* and δ are shown in Fig. 14. Also, the effects of mass transfer and slip on the pressure distribution are shown in Fig. 15. At zero injection, the effects of slip on the pressure distribution became negligibly small as $x \to 1$.

The skin-friction coefficient, C_{f_∞}, and Stanton number, St_∞, are shown in Figs. 16a and b, respectively. The results with mass transfer and slip are shown, and the effects of viscous interaction and transverse curvature were included in the calculations. In accord with the previously discussed results with slip, the effects of C_{f_∞} and St_∞ were substantially reduced as x increased; however, it is interesting to note that the effects of slip were somewhat greater on St_∞ than on C_{f_∞}, whereas the effects of mass transfer on the two coefficients were nearly equal.

Comparisons of experimental pressure data and theoretical predictions are shown in Fig. 17. The uncorrected experimental data are indicated with flagged symbols. The data were corrected for orifice size after Potter, Kinslow, and Boylan (Ref. 13), and those results are also shown. The predictions from the present investigations are shown, and for comparison the inviscid sharp cone values and the free-molecule values after Hayes and Probstein (Ref. 14) are also shown. The present iterated flow field and free-molecule flow predictions both overestimate the measured surface pressure. As noted earlier, the orifice correction is large and the experimental uncertainty is currently unknown. The trends of both the uncorrected and corrected surface pressure data are as expected, i.e., the pressure tends toward the free-molecule value as $x \to 0$. The agreement between experimental data and numerical results is encouraging; however, further work is required to better define the experimental uncertainty and correction factors (orifice size and thermal transpiration) as well as the applicability of the theoretical model at these low Reynolds number conditions.

It is also worth noting that the difference between the inviscid sharp cone value and the free-molecule value is primarily due to the large wall-to-free-stream temperature ratio. The wall temperature effect increases with increasing T_w/T_∞ (see Hayes and Probstein, Ref. 14).

---

*Hereafter slip will be used to denote both slip and temperature jump effects.

Comparisons of the experimental drag data at $M_\infty \sim 10$ with the predictions from the present investigation are shown in Fig. 18. The effects of mass transfer, viscous interaction, transverse curvature, matching conditions, slip, and temperature jump are indicated. Only the final converged solutions are shown except at the lowest Reynolds number. The results of each iteration and the combined effects of mass transfer and slip at the lowest Reynolds number are shown in Fig. 19 to indicate the large changes in the total drag between iterations. The effect of the term $\rho_w v_w r_w / \rho_e u_e r_e$ on the matching condition with and without slip is also shown in the figure. The effect of the term on the total drag was about 5 percent and in a direction away from the experimental results.

It is interesting to note that for the same total mass flow rate, $\dot{m}$, the effects of injection on the drag increase with decreasing Reynolds number. This is also in agreement with the experimental results of Whitfield and Griffith (Ref. 2) for the case of tangential injection. It thus appears that the effects of mass transfer (either normal or tangential) are more important on inviscid-viscous flow fields under low Reynolds number conditions.

In considering the comparison of numerical results and experimental data with mass transfer, the basic deficiency in the theoretical model should be remembered. Uniform mass transfer was assumed over the entire cone, whereas in the AEDC-VKF experiments the forward 32.5 percent of the cone surface area was impervious to mass transfer. Moreover a theoretical model with impervious nose and porous afterbody would probably predict an increase in total drag because of (1) an increase in pressure and friction drag over the impervious nose and (2) an increase in pressure drag over the porous afterbody. It is not clear whether the friction drag would be increased or decreased over the porous region since the increased mass flux would tend to reduce the skin friction; however, the thicker boundary layer would tend to increase the viscous and transverse-curvature-induced friction drag. Therefore considering the deficiency in the theoretical model with regard to nonuniform mass transfer distributions, the results of the present predictions are considered to be satisfactory.

A comparison of numerical results and experimental data for all the zero-lift drag data without mass transfer is shown in Fig. 20. For comparison, the previously published experimental data of Whitfield and Griffith are also shown. The drag data are shown against the

hypersonic interaction parameter $\bar{v}_\infty \equiv M_\infty (C_\infty/Re_{\infty,})^{1/2}$ proposed by Whitfield and Griffith.* In general, the numerical results based on the matching condition v_e/u_e and including slip agree with the experimental data within experimental uncertainty.

SECTION V
CONCLUDING REMARKS

When the theoretical model developed in the present report was used to predict the viscous-induced pressure increment and zero-lift drag of a sharp, 5-deg half-angle cone at the Berkeley conditions (M_∞ = 3.93 and 5.64), the results were in better agreement with the experimental data than were the previous analytical results of King and Talbot (Refs. 5 and 6). This was especially true for the effects of mass transfer on the total drag at moderately high injection rates.

The same theoretical model was used to predict viscous effects on a 9-deg half-angle cone at M_∞ = 9.37 and 10 over a range of Reynolds numbers and wall-to-stagnation temperature ratios. At zero injection, in general the predictions of zero-lift drag agreed with the experimental data within experimental uncertainty. However with injection, the basic deficiency of the theoretical model, viz., neglecting the effects of a large impermeable nose, was more important. The effects of inviscid-viscous flow field matching conditions, slip, and temperature jump as applied in the present report were found to have a significant effect on viscous-induced pressure and friction drag increments. The comparison of experimental and predicted surface pressures showed substantial disagreement, and the need for further investigation is indicated. Without mass transfer the theoretical model of this report is applicable to arbitrary, pointed, two-dimensional, and axisymmetric bodies as long as boundary-layer theory is applicable and an inviscid outer flow exists which can be approximated by tangent wedge or cone theory. Under the rarefied flow conditions at M_∞ = 10 considered in this report, the above-noted requirements might not have been met. However, the comparisons shown are encouraging, and further experiments and numerical studies are required to better define the effects of wall-to-stagnation temperature ratio and wall temperature distributions and the nature of the outer flow field and shock wave.

---

*Some additional comments and a derivation of the parameter $\bar{v}_\infty$ are given by Lewis and Whitfield (Ref. 3).

REFERENCES

1. Griffith, B. J. and Lewis, C. H. "Laminar Heat Transfer to Spherically Blunted Cones at Hypersonic Conditions." AIAA J., Vol. 2, 1964, pp. 438-444.

2. Whitfield, J. D. and Griffith, B. J. "Hypersonic Viscous Drag Effects on Blunt Slender Cones." AIAA J., Vol. 2, 1964, pp. 1714-1722.

3. Lewis, C. H. and Whitfield, J. D. "Theoretical and Experimental Studies of Hypersonic Viscous Effects." AGARDograph 97, Part III, 1965, pp. 63-119. Also AEDC-TR-65-100 (AD462717), 1965.

4. Little, H. R. and Griffith, B. J. "Drag of Slender Cones at Hypersonic Mach Numbers with Film and Transpiration Cooling." AEDC-TR-66-9, to be published.

5. King, H. H. "Hypersonic Flow over a Slender Cone with Gas Injection." University of California (Berkeley) TR-HE-150-205, 1962.

6. King, H. H. and Talbot, L. "Effect of Mass Injection on the Drag of a Slender Cone in Hypersonic Flow." AIAA J., Vol. 2, 1964, pp. 836-844.

7. Low, G. M. "The Compressible Laminar Boundary Layer with Fluid Injection." NACA TN 3404, 1955.

8. Yasuhara, M. "Axisymmetric Viscous Flow Past Very Slender Bodies of Revolution." J. Aerospace Sci., Vol. 29, 1962, pp. 667-679, 688.

9. Clutter, D. W. and Smith, A.M.O. "Solution of the General Boundary Layer Equations for Compressible Laminar Flow, Including Transverse Curvature." Douglas Aircraft Company Report LB 31088, 1963; revised 1964. See also AIAA J., Vol. 3, 1965, pp. 639-647.

10. Li, T-Y. and Gross, J. F. "Transverse Curvature Effects in Axisymmetric Hypersonic Boundary Layers." AIAA J., Vol. 2, 1964, pp. 1868-1869.

11. Van Dyke, M. "Second-Order Compressible Boundary Layer Theory with Application to Blunt Bodies in Hypersonic Flow." In Hypersonic Flow Research (ed. by F. R. Riddell), Academic Press, New York, 1962, pp. 37-76.

12. Pan, Y. S. and Probstein, R. F. "Rarefied Flow Transition at a Leading Edge." MIT Fluid Mech. Lab Publication 648, 1964.

13. Potter, J. L., Kinslow, M., and Boylan, D. E. "An Influence of the Orifice on Measured Pressures in Rarefied Flow." Paper given at the 4th International Symposium on Rarefied Gas Dynamics, Toronto, Canada, July 1964.

14. Hayes, W. D. and Probstein, R. F. Hypersonic Flow Theory. Academic Press, New York, 1959, Chap. 10, p. 401.

15. Mann, W. M., Jr. "Effective Displacement Thickness for Boundary Layers with Surface Mass Transfer." AIAA J., Vol. 1, 1963, pp. 1181-1182.

16. Thyson, N. A. and Schurmann, E.E.H. "Blowing Effects on Pressure Interaction Associated with Cones." AIAA J., Vol. 1, 1963, pp. 2179-2180.

17. Davis, R. T. and Flügge-Lotz, I. "Second-Order Boundary Layer Effects in Hypersonic Flow Past Axisymmetric Blunt Bodies." J. Fluid Mech., Vol. 20, 1964, pp. 593-623.

18. Li, J. M. and Street, R. E. "The Incipient Continuum Flow near the Leading Edge of a Flat Plate." Paper given at 4th International Symposium on Rarefied Gas Dynamics, Toronto, Canada, July 1964.

19. Street, R. E. "The Study of Boundary Conditions in Slip-Flow Aerodynamics." In Rarefied Gas Dynamics (ed. by F. M. Devienne), Pergamon Press, New York, 1960, pp. 276-292.

APPENDIX I
INVISCID-VISCOUS FLOW FIELD MATCHING CONDITIONS

The effects of mass transfer on inviscid-viscous flow field matching conditions have been considered by Mann (Ref. 15) and Thyson and Schurmann (Ref. 16). More recently, Li and Gross (Ref. 10) considered the combined effects of mass transfer and transverse curvature by integrating the continuity equation from $y = 0$ to $y = \delta(x)$. In so doing they obtained the following matching conditions for a sharp cone in hypersonic flow:

$$\frac{v_e}{u_e} = \frac{\rho_w v_w r_w}{\rho_e u_e r_e} + \frac{d\delta}{dx}\left(1 - \frac{r_w}{r_e}\right) + \frac{r_w}{r_e}\left[\frac{d\delta^*}{dx} - \frac{\delta - \delta^*}{\rho_e u_e r_e}\frac{d}{dx}(\rho_e u_e r_w)\right] - \cos\theta_c\left[\frac{\delta^2 - \delta^{*2}}{2\rho_e u_e r_e}\frac{d(\rho_e u_e)}{dx} - \frac{1}{r_e}\left(\delta\frac{d\delta}{dx} - \delta^*\frac{d\delta^*}{dx}\right)\right] \quad \text{(I-1)}$$

Li and Gross then state "... In hypersonic boundary layers, $\delta^* \to \delta$; then Eq. (I-1) becomes

$$\frac{v_e}{u_e} = \frac{\rho_w v_w r_w}{\rho_e u_e r_e} + \frac{d\delta^*}{dx} \quad \text{(I-2)}$$

(which) provides the necessary condition ..."

For two of the conditions studied in the present report, the following data were obtained from the zeroth iteration without mass transfer at $x = 0.90$:

M_∞	Re_∞/in.	θ_c, deg	T_w/T_o	δ^*/δ	$\tan^{-1}(d\delta^*/dx)$, deg	$\tan^{-1}(v_e/u_e)$, deg
5.64	6200	5	0.96	0.78	1.68	1.01
10.0	396	9	0.20	0.71	4.12	1.97

The effect of the terms neglected by Li and Gross under the hypersonic approximation caused a 40- and 50-percent change in $\tan^{-1}(d\delta^*/dx)$ at $M_\infty = 5.64$ and 10, respectively. This corresponds to a reduction of the viscous-induced pressure term $p/p_{inv} - 1$ of 39 and 56 percent at $M_\infty = 5.64$ and 10, respectively. It therefore appears significant and desirable to evaluate the complete Eq. (I-1) rather than using the hypersonic approximation and the resulting Eq. (I-2).

The effect of the term $\rho_w v_w r_w/\rho_e u_e r_e$ in Eq. (I-2) was investigated at $M_\infty = 10$ and Re_∞/in. = 396 where the effect on v_e/u_e was a maximum.

Under those conditions, the effect on total drag was about 5 percent. Therefore for more direct comparison with King and Talbot,

$$v_e/u_e = d\delta^*/dx \qquad \text{(I-3)}$$

was used in most of the calculations. The inviscid flow field was computed from the approximate tangent cone theory. The pressure on the effective cone of half-angle $\theta_{eff} = \theta_c + \tan^{-1}(v_e/u_e)$ was determined according to either Eq. (I-1) or (I-3), and matching is denoted v_e/u_e or $d\delta^*/dx$, respectively.

APPENDIX II
ITERATION SCHEME

In order to consider the coupled effects of the various second-order terms including viscous interaction, it was necessary to iterate successive boundary-layer solutions until a converged solution was obtained. Regardless of whether the matching condition was based on $d\delta^*/dx$ or v_e/u_e, it was difficult to obtain sufficiently smooth pressure and velocity distributions. Three-point numerical differentiation of $\delta(x)$ and $\delta^*(x)$ was satisfactory at the lower Mach numbers, $M_\infty = 3.93$ and 5.64, but was unsatisfactory at $M_\infty = 9.37$ and 10 since small variations in the smoothness of the θ_{eff} profile, inherent in the numerical differentiation scheme, caused appreciable oscillations in succeeding boundary-layer solutions. Several schemes for fitting $\delta(x)$ and $\delta^*(x)$ with polynomials were tried, and although good fits of the profiles were obtained the corresponding analytical derivatives were poorly behaved.

The δ and δ^* calculated data were fitted with a power law and exponential equation of the form

$$\delta = ax^b - \exp(cx - d)$$

This equation fitted the data well (average error about ±0.2 percent) for the majority of the cases considered. Also, the resulting derivative

$$d\delta/dx = abx^{b-1} - c \exp(cx - d)$$

was well behaved. However, this form of equation characteristically gave a poor solution near $x = 0$, and to account for this, θ_{eff} was graphically extrapolated over the region $0 \leq x \leq 0.1$. This gave reasonable values of pressure and velocity for starting the solution and had a negligible effect on the total zero-lift drag since only 1 percent of the cone surface area was within the extrapolated region.

For the cases with mass transfer at the wall, the problem was further complicated. Solutions based on the experimental injection laws (at $M_\infty \sim 10$ injection started at $x = 0.57$) proved impossible to iterate by the method of successive approximations since the rapid changes in $d\delta^*/dx$ encountered near the start of the injection region induced serious oscillations into the solution. In the cases which were iterated, the mass flux was computed from $\rho_w v_w = \dot{m}/A_w$, where $\dot{m}$ is the total (experimental) mass transfer rate and A_w is the total surface area of the cone. The resulting average mass flux was assumed constant over the entire surface of the cone. This eliminated the oscillations and permitted inviscid-viscous flow field iterations to be made. When the mass flux reached a sufficiently large value, boundary-layer "blow-off" ($f''_w \to 0$)

occurred on the cone. It was possible, however, to obtain iterated flow field solutions at moderately high injection rates if the rapid increase in $\delta(x)$ and $\delta^*(x)$ as $x \to 1$ was ignored. This is justified on the basis that the corresponding viscous-induced pressure acts to reduce a rapid increase in $\delta^*(x)$. It is also noted that each calculation is to be considered as an iterate or approximate solution to the final converged solution, and thus an exact fit of $\delta^*(x)$ was not necessarily the most desirable for each successive approximation at moderately high blowing rates.

With the "effective" body obtained as described above, the "effective" cone angle θ_{eff} and matching condition $d\delta^*/dx$ or v_e/u_e were used with the ideal gas ($\gamma = 1.4$) tangent cone solutions to determine $p_e(x)$ and $u_e(x)$. The boundary-layer calculations then proceeded in the usual manner.

APPENDIX III
SLIP AND TEMPERATURE JUMP CONDITIONS

The effects of slip and temperature jump at the surface of blunt-nosed bodies have been studied by several investigators in recent years (see, e.g., Refs. 11 and 17). Recently Pan and Probstein (Ref. 12) and Li and Street (Ref. 18) have considered an impermeable, semi-infinite flat plate under rarefied flow conditions. The results of the latter investigations varied greatly on the prediction of the beginning of the region of continuum, strong interaction plus wall slip and temperature jump. Moreover, most authors have evaluated the mean free path at the wall conditions, say T_w and p_w, rather than at the slip conditions $T(\eta = 0)$ and p_w. This usual procedure was also used in the present report but is not a necessary condition for the numerical calculations.

The wall slip velocity and temperature jump were computed according to the formulas given by Street (Ref. 19) and Van Dyke (Ref. 11):

$$u(0) = (\mu R/p)\left[(\pi T/2R)^{1/2}\,\partial u/\partial y + (3/4)\,\partial T/\partial x\right] \tag{III-1}$$

$$T(0) = T_w + (\mu R/p)\,(15/8)\,(\pi T/2R)^{1/2}\,\partial T/\partial y \tag{III-2}$$

where the right-hand sides of both equations were evaluated at the wall conditions, the hard sphere model was used to evaluate constants in both formulas, and the reflection and thermal accommodation coefficients were assumed to be unity.

Under the transformations used by Clutter and Smith (Ref. 9),

$$x = x \text{ and } \eta = (u_e L/\rho_* u_* x)^{1/2} \int_0^r \rho\, dy \tag{III-3}$$

Eqs. (III-1) and (III-2) become, respectively,

$$f'(\eta = 0) = \frac{\mu_w}{p_w}\frac{1}{L}\left[\left(\frac{\pi}{2}\frac{\gamma-1}{\gamma} h_w\, Re_{*,L}\,\frac{u_e}{u_*}\frac{1}{x}\right)^{1/2}\frac{\rho_w}{\rho_*} f''_w + \frac{3}{4}\frac{\gamma}{\gamma-1}\frac{u_*}{u_e}\frac{h_{ref}}{u_*}\frac{\partial}{\partial x}\left(\frac{h}{h_{ref}}\right)_w\right] \tag{III-4}$$

$$h(\eta = 0) = h_w + \frac{15}{8}\frac{\mu_w}{p_w}\left(\frac{\pi}{2}\frac{\gamma-1}{\gamma} h_w\, Re_{*,L}\,\frac{u_e}{u_*}\frac{1}{x}\right)^{1/2}\frac{\rho_w}{\rho_*}\frac{1}{L}\left(\frac{\partial h}{\partial \eta}\right)_w \tag{III-5}$$

The local skin-friction coefficient

$$Cf_* \equiv 2\,\tau_w/\rho_* u_*^2 = 2(u_e/u_*)^{3/2}\,(1/x)\,(\rho_w\mu_w/\rho_*\mu_*)\,f''_w$$

is not altered because of slip and temperature jump; however, the heat-transfer rate to the surface becomes

$$q_w = [(\mu/Pr)\ \partial h/\partial y + \mu u\,(\partial u/\partial y)]_w$$

and with the Stanton number defined

$$St_* \equiv q_w/\rho_* u_* (H_e - h_w)$$

the ratio St_*/C_{f_*} becomes

$$\frac{St_*}{C_{f_*}} = \frac{1}{2(1-g_w)} \frac{u_*}{u_e} \left[\frac{1}{Pr} \frac{g'_w}{f''_w} + \frac{u_e^2}{H_e} f'_w \left(1 - \frac{1}{Pr}\right) \right] \qquad \text{(III-6)}$$

The Clutter-Smith theory (Ref. 9) was modified to include Eqs. (III-4), (III-5), and (III-6). However, before sharp-nosed body calculations could be made it was necessary to consider the effects of the singularity at $x = 0$. The order of the singularity for a pointed body is such as to preclude internally consistent calculations at that point. However, the boundary-layer equations are not applicable at $x = 0$ and a small region near $x = 0$ was in near free-molecule flow. The extent of the noncontinuum region for a sharp cone in rarefied flow has not been investigated. However, Pan and Probstein have considered the problem for a sharp flat plate, and their estimates for the conditions of the present investigation are of interest.

Pan and Probstein gave the criterion $Re_{\infty,x_i}/M_\infty \simeq 8$ for the beginning of the "boundary layer plus normal pressure gradient" region. This region lies downstream of the near free-molecule and transition regions and upstream of the hypersonic strong interaction region (see Ref. 12). The region was treated by Pan and Probstein as continuum flow with wall slip and temperature jump, and they investigated the effects of slip, curvature, and thickness of the shock wave in addition to the effects of the normal pressure gradient. (In the present report all transport effects on the shock wave and the normal pressure gradient effects were ignored.)

Using the Pan and Probstein criterion,

$$\frac{x_i L}{\lambda_\infty} = \frac{Re_{\infty,x_i}}{M_\infty} \frac{1}{C_\infty M_\infty} \frac{2}{\gamma - 1} \left(\frac{T_0}{T_w} \frac{\gamma + 1}{\gamma} \frac{1}{\pi} \right)^{1/2}$$

with $Re_{\infty,x_i}/M_\infty = 8$, for the Tunnel L conditions the initial location x_i was computed as follows:

TUNNEL L

M_∞	Re_∞/in.	T_w/T_o	λ_∞, in.	$x_i L/\lambda_\infty$	x_i
9.37	2869	0.6	0.0048	7.0	0.011
9.37	1632	0.4	0.0085	5.5	0.021
10	396	0.2	0.037	6.8	0.105

One thus sees that except at the lowest Reynolds number, the noncontinuum region was very small in extent. Pan and Probstein also predicted that the region of strong viscous interaction plus slip should begin at $Re_{\infty,x}/M_\infty \simeq 40$ to 45. Thus at the lowest Reynolds number approximately one-half of the cone was within the (flat-plate) noncontinuum and boundary-layer plus normal pressure gradient regions. For the other conditions no more than 0.125 of the length or 0.0156 of the area of the cone was upstream of the (flat-plate) strong interaction region. Also without slip the strong interaction region of a cone is much less than for a flat plate.

Therefore in the present study the noncontinuum and boundary layer plus normal pressure gradient regions were neglected. The boundary-layer solutions with slip and temperature jump were begun as near $x = 0$ as practical (usually at $x \sim 0.025$) using the modified Clutter-Smith theory and the tangent cone theory. The calculations were started from the converged no-slip solutions. At x_i the nonsimilar terms (e. g., $\partial f'/\partial x$, $\partial g/\partial x$) in the momentum and energy equations were set to zero. However, the transverse curvature term, which in the original Clutter-Smith machine program was also set to zero at the initial station, was retained in the modified theory. The boundary layer with slip and temperature jump was also iterated as the no-slip solutions were, and the method of iteration is discussed in Appendix II.

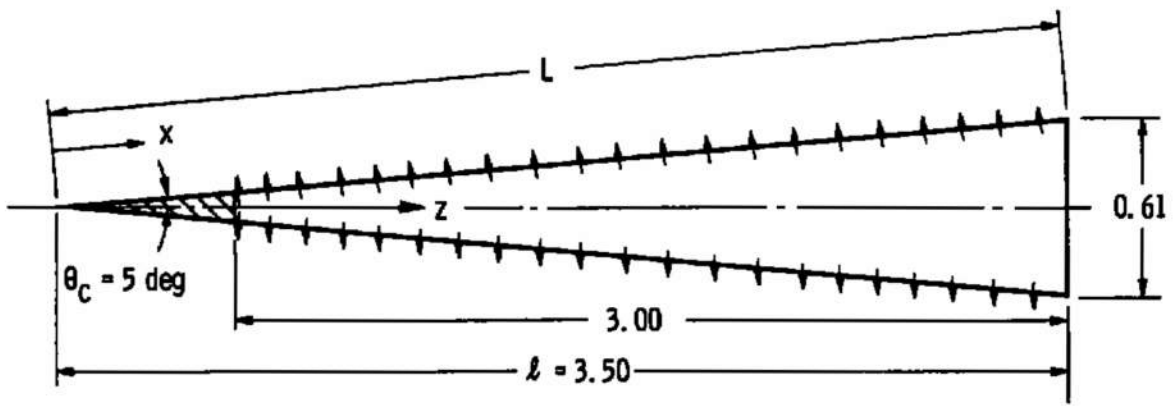

All Dimensions in Inches

a. Berkeley Low Density Tunnel Force Model

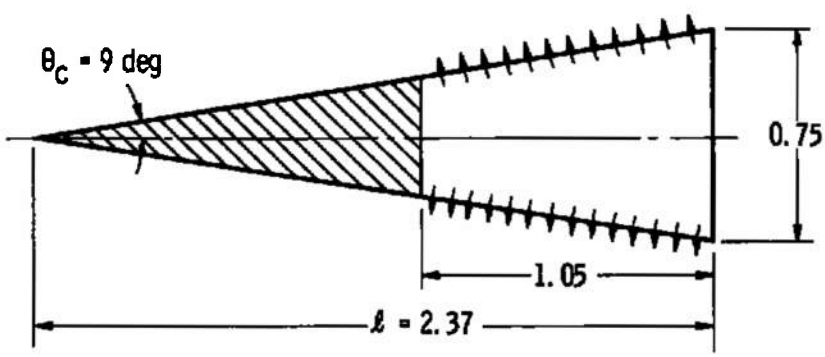

All Dimensions in Inches

b. AEDC-VKF Force Model

Fig. 1 Force, Pressure, and Wall Temperature Models

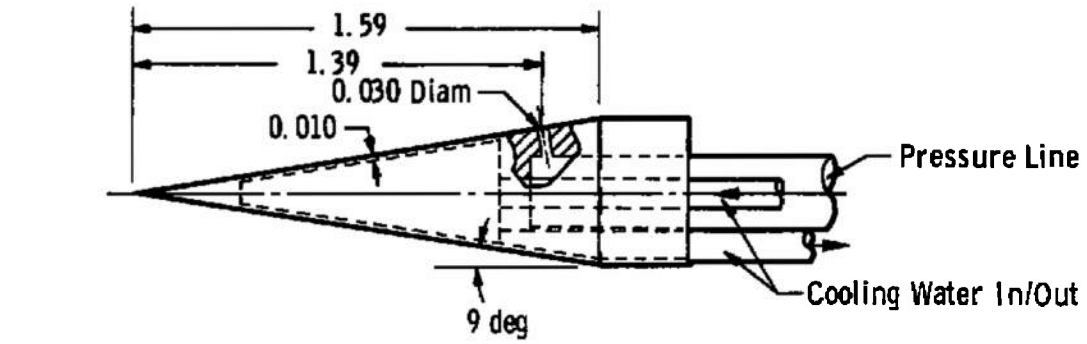

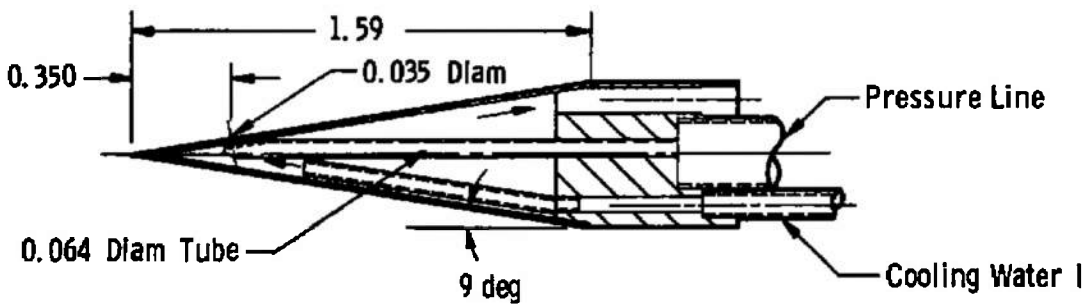

c. AEDC-VKF Pressure Models

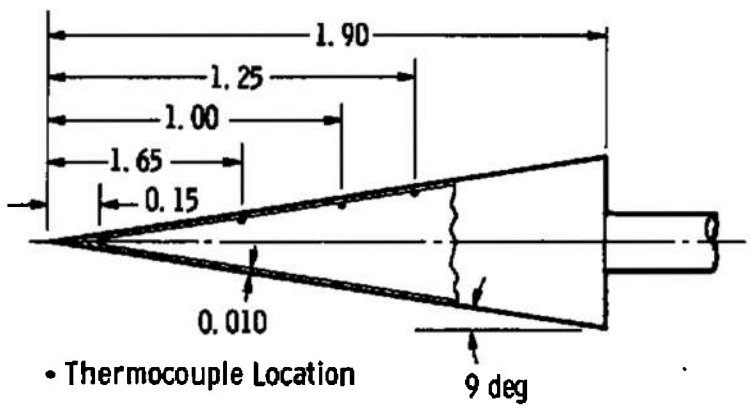

All Dimensions in Inches

d. AEDC-VKF Wall Temperature Model

Fig. 1 Concluded

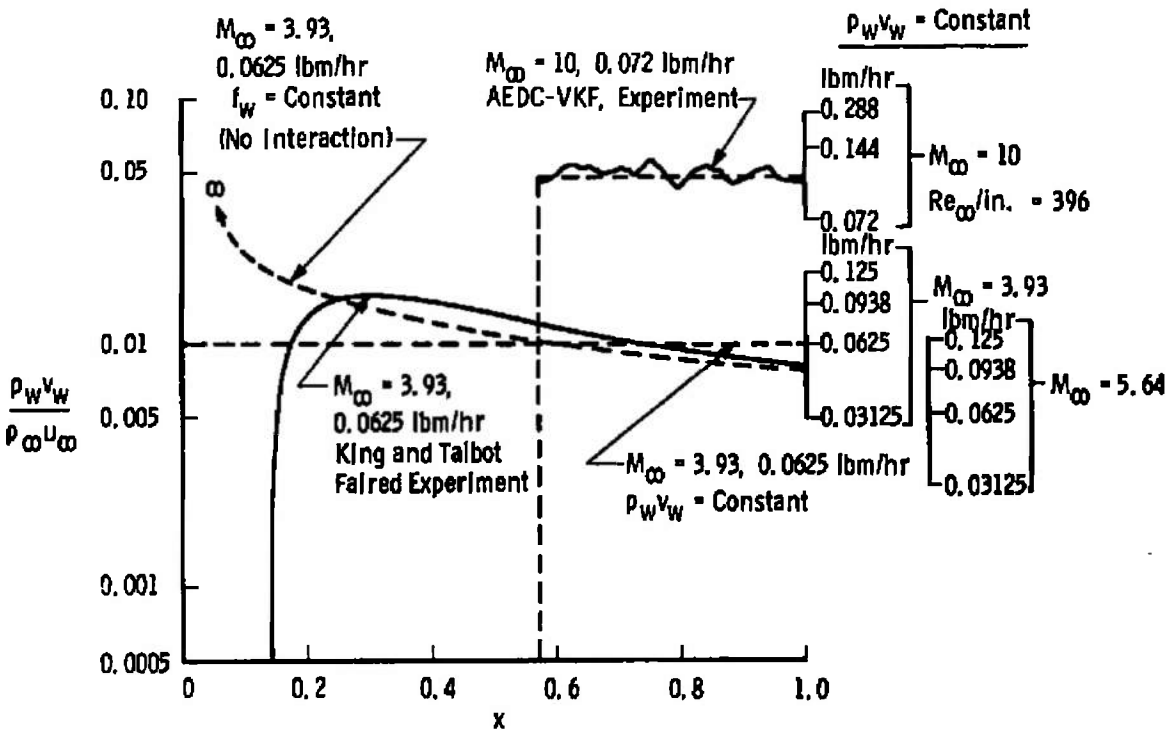

Fig. 2 Comparison of Gas Injection Laws

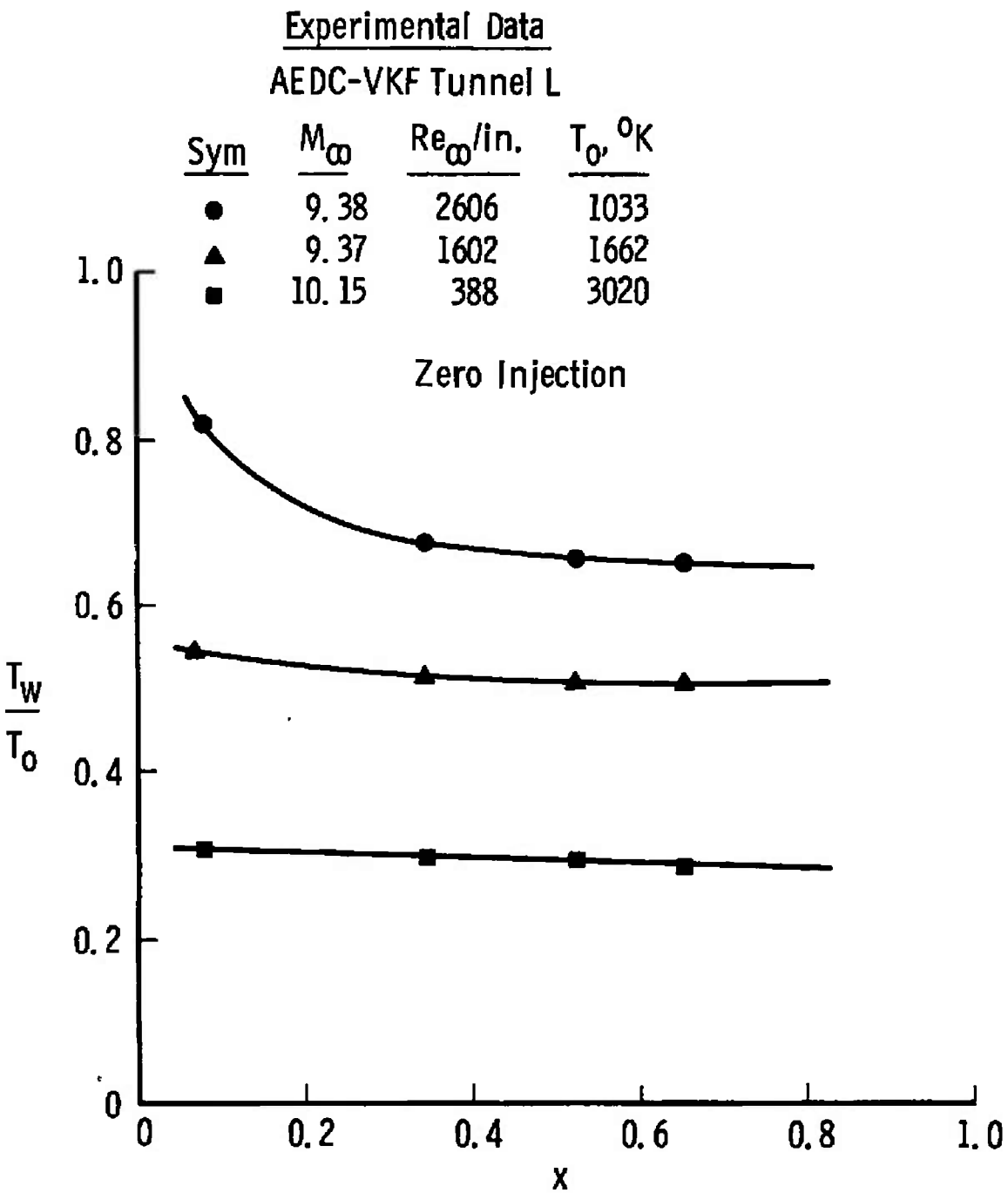

Fig. 3 Equilibrium Wall Temperature Distributions over a Hallow 9-deg Half-Angle Cone

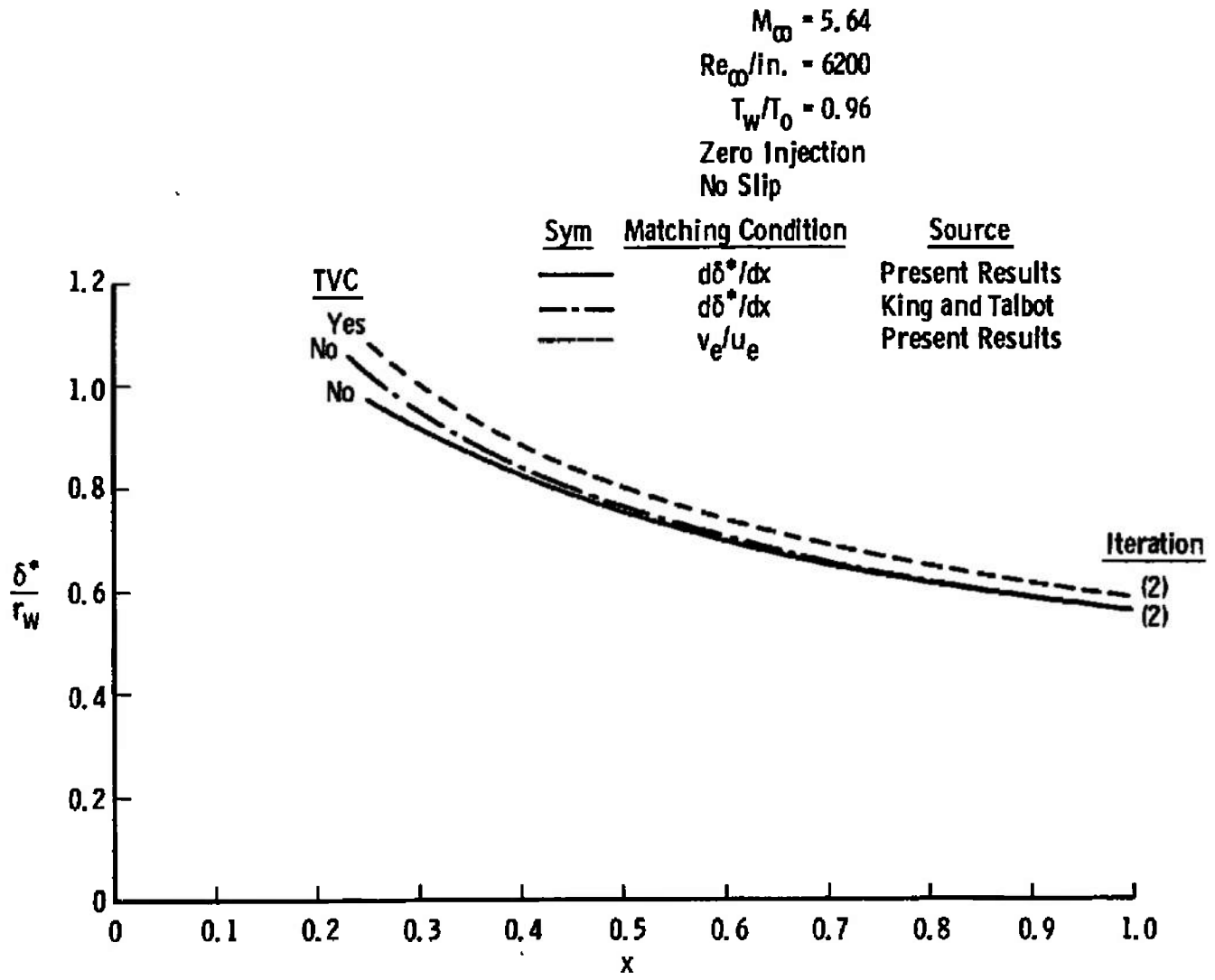

Fig. 4 Boundary-Layer Displacement Thickness over a 5-deg Half-Angle Cone

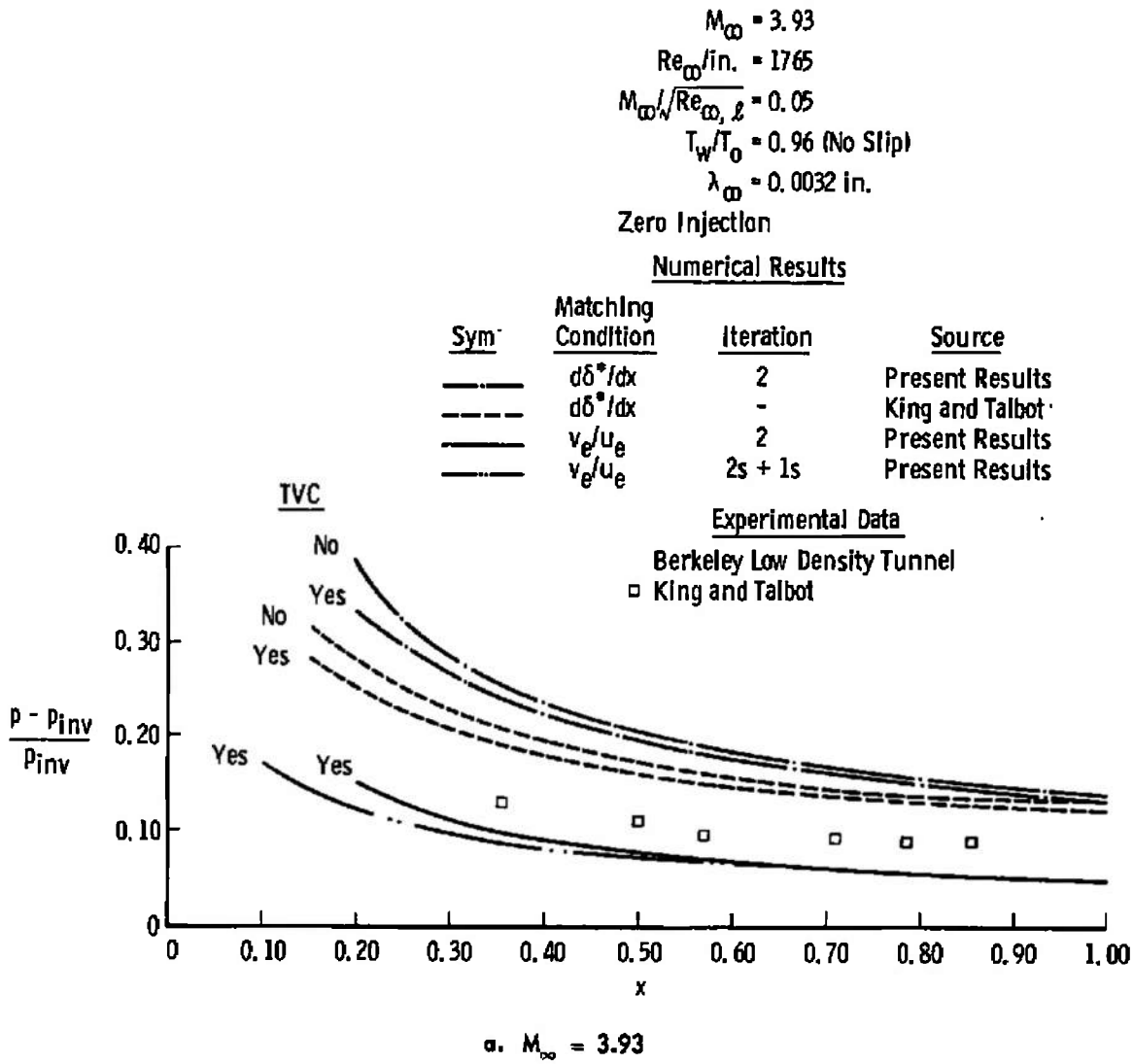

a. M_∞ = 3.93

Fig. 5 Effects of Viscous Interaction and Transverse Curvature on Sharp Cone Pressure Distribution

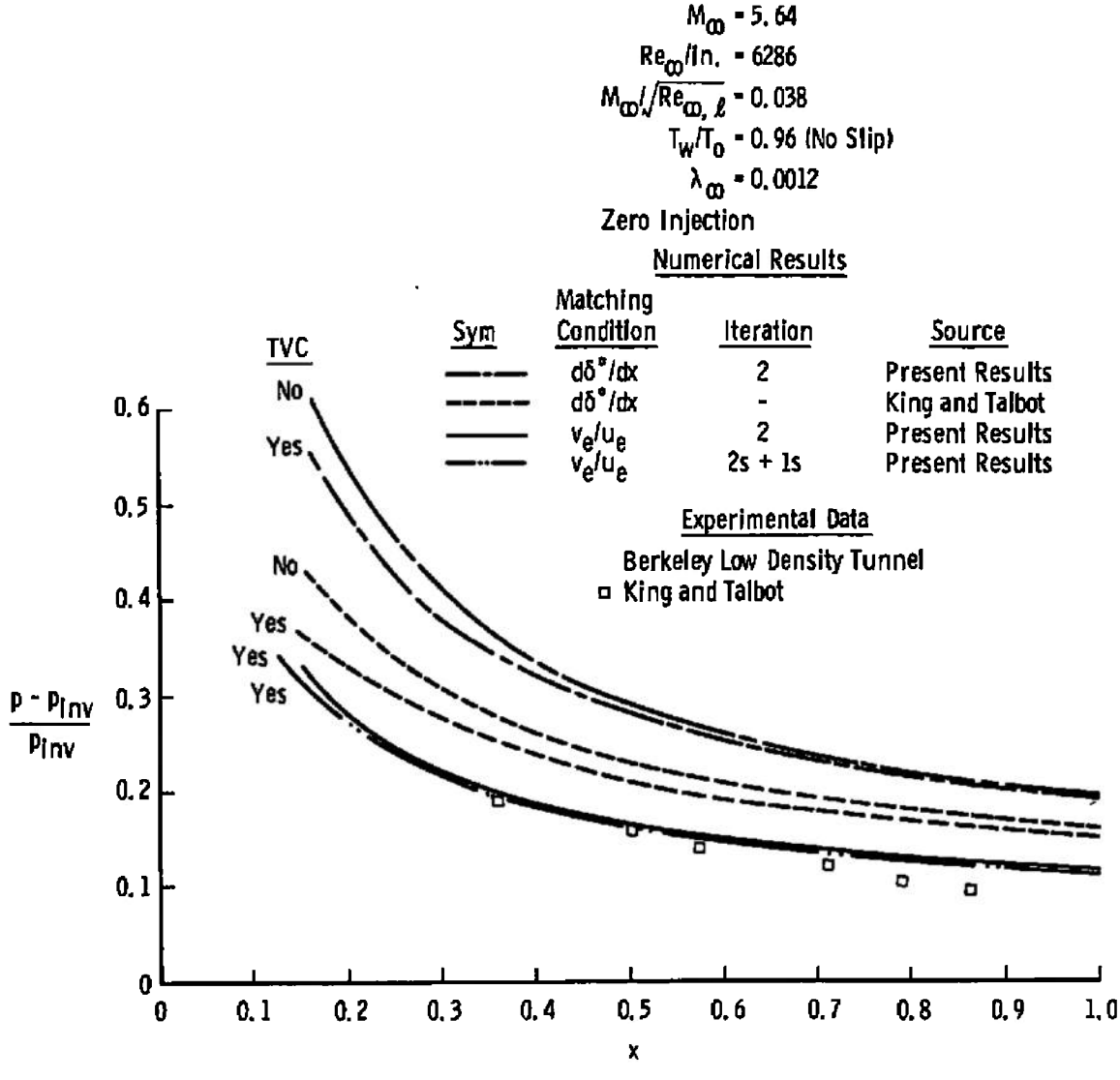

b. M_∞ = 5.64

Fig. 5 Concluded

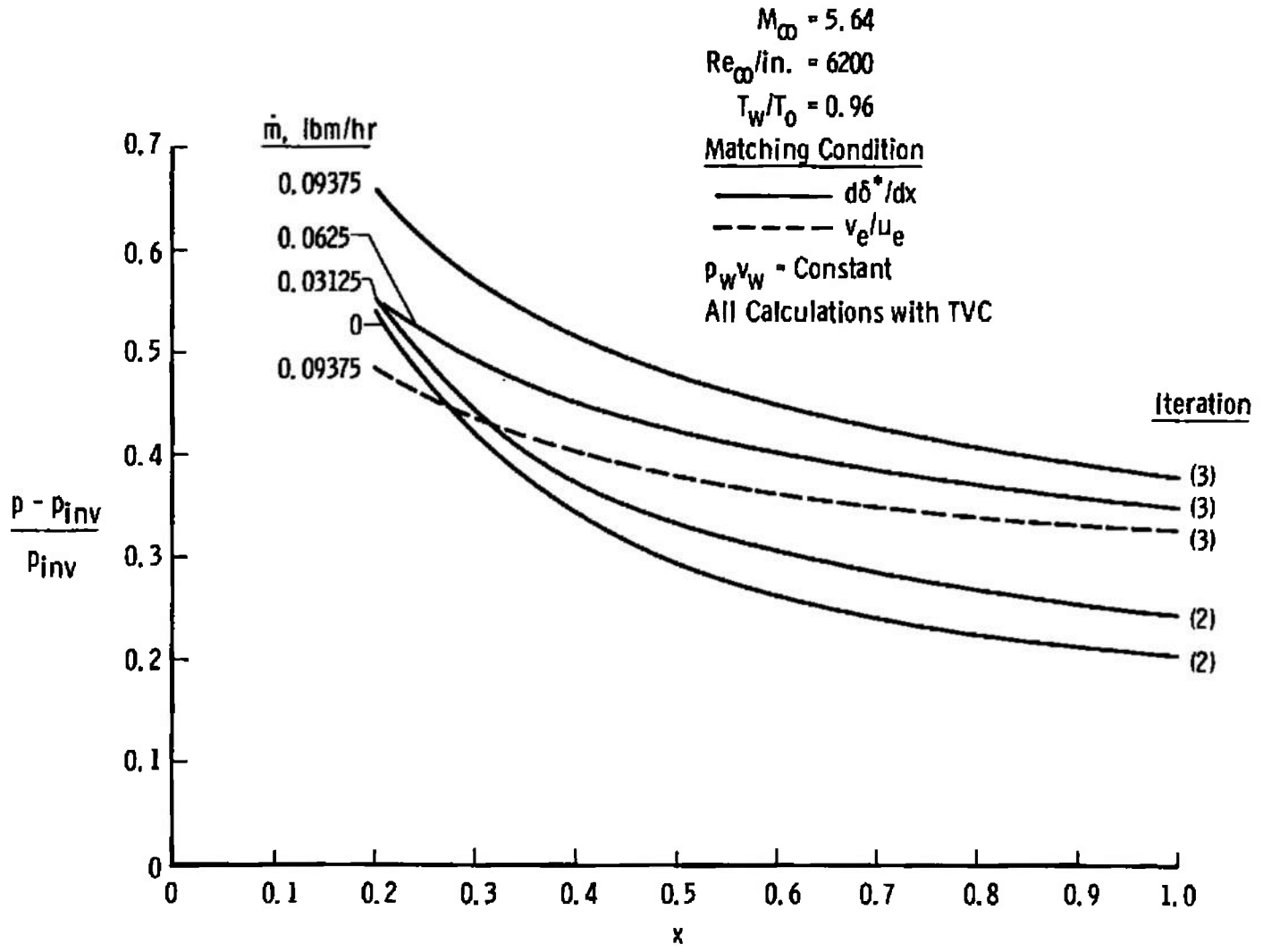

Fig. 6 Effects of Mass Transfer and Viscous Interaction on a 5-deg Half-Angle Cone at M_∞ = 5.64

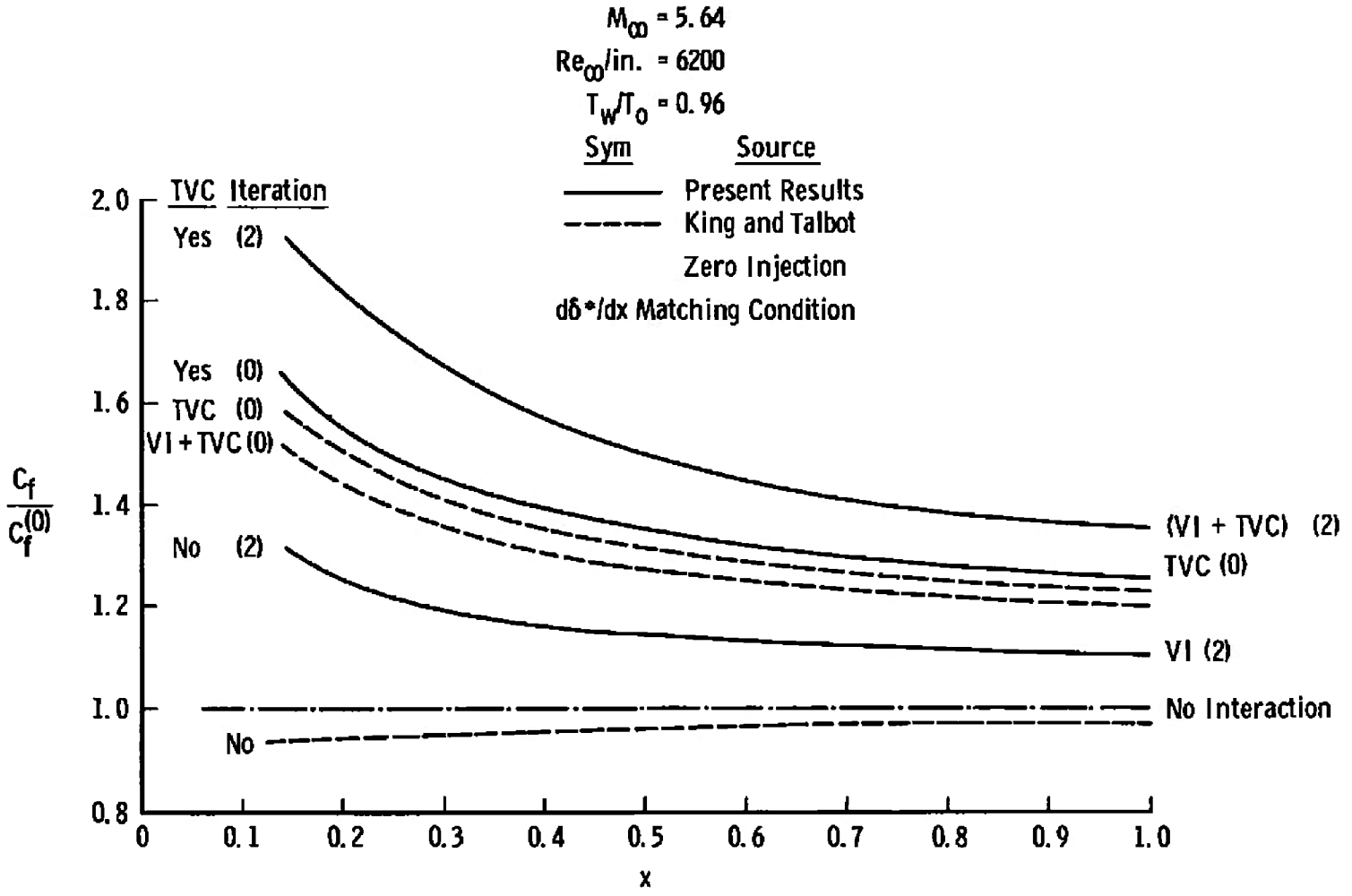

Fig. 7 Effects of Viscous Interaction and Transverse Curvature on Skin-Friction Coefficient

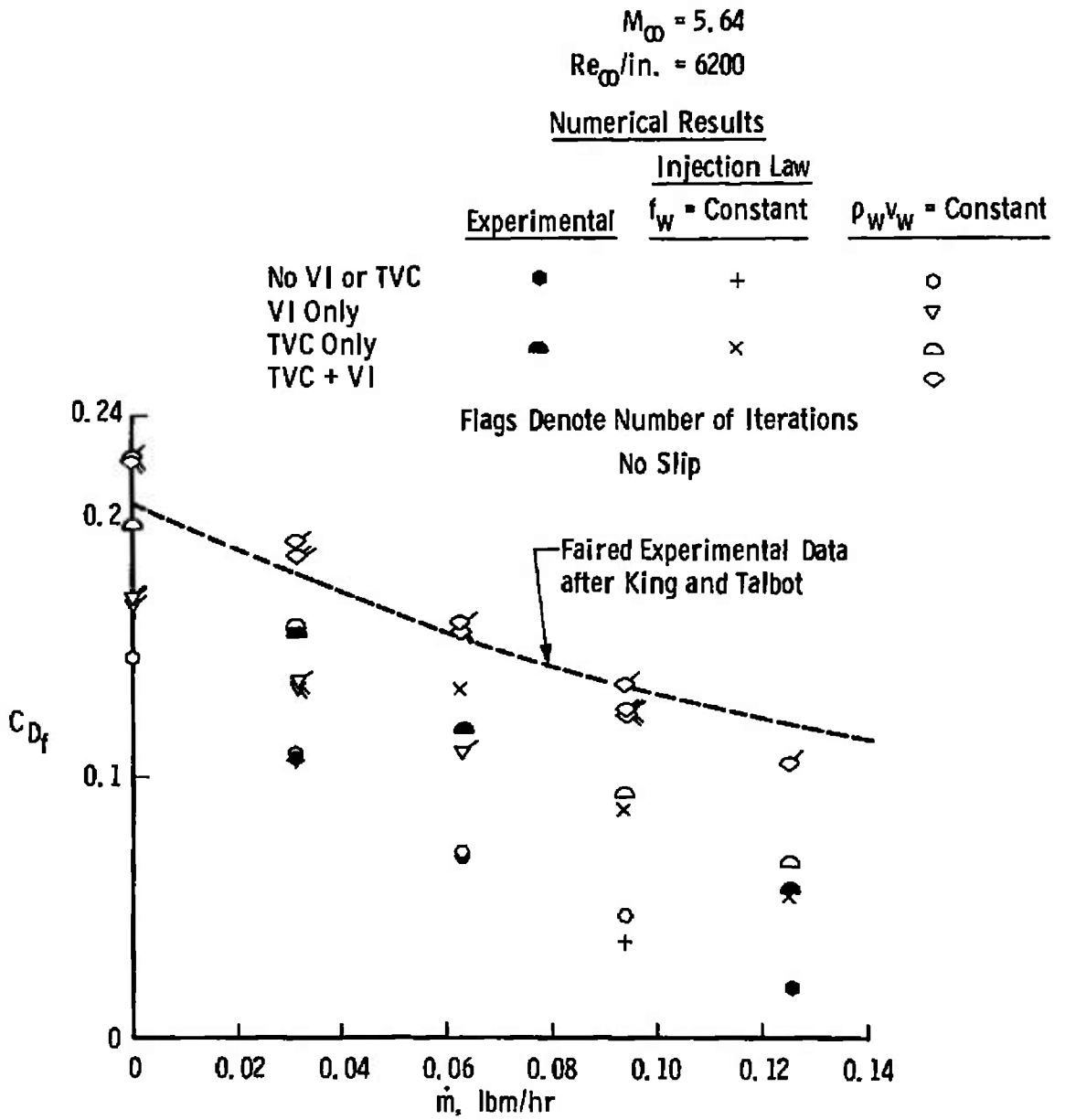

Fig. 8 Effects of Various Injection Laws on Friction Drag Coefficient

$M_\infty = 3.93$
$Re_\infty/in. = 1765$
$T_w/T_o = 0.96$ (No Slip)

Experimental Data
Berkeley Low Density Tunnel
——— King and Talbot

Sym	Matching Condition	Numerical Results: Injection Law	Source
— — —	$d\delta^*/dx$	$\rho_w v_w$ = Const.	Present Results
— — — —	$d\delta^*/dx$	f_w = Const.	King and Talbot
△	v_e/u_e	$\rho_w v_w$ = Const.	Present Results

Flag Denotes Slip

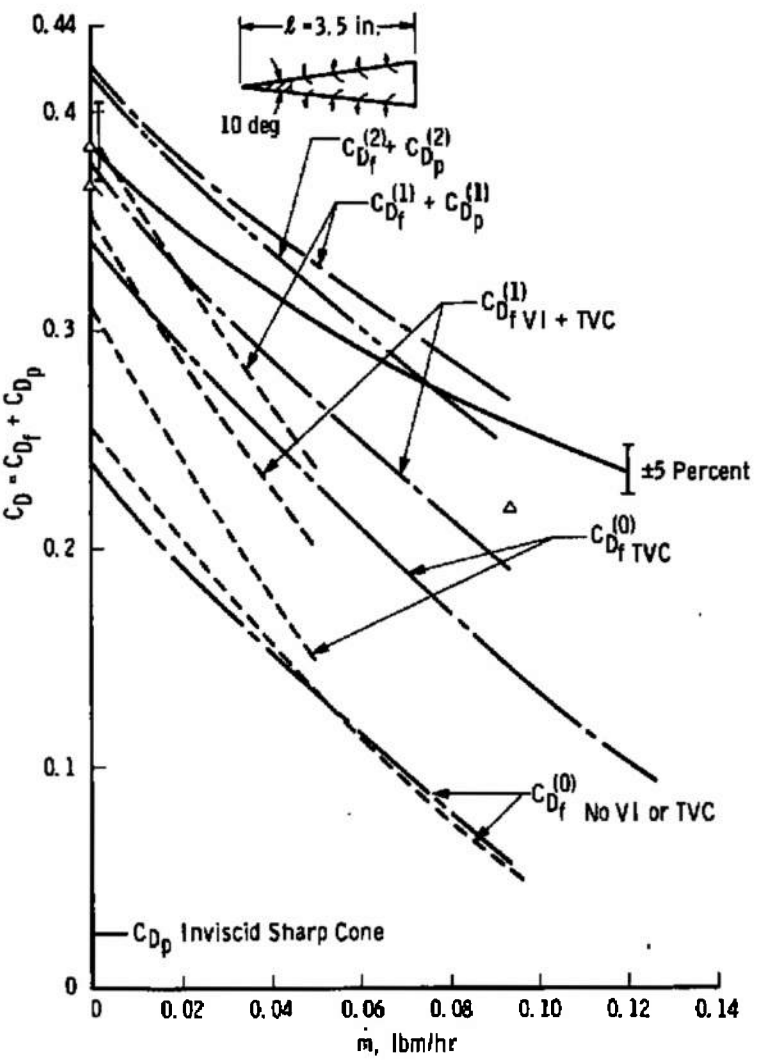

a. $M_\infty = 3.93$

Fig. 9 Drag Components

$M_\infty = 5.64$
$Re_\infty/in. = 6200$
$T_w/T_0 = 0.96$ (No Slip)

Experimental Data

Berkeley Low Density Tunnel
—— King and Talbot

Numerical Results

Sym	Matching Condition	Injection Law	Source
———	$d\delta^*/dx$	$\rho_w v_w$ = Const.	Present Results
———	$d\delta^*/dx$	f_w = Const.	King and Talbot
△	v_e/u_e	$\rho_w v_w$ = Const.	Present Results

Flag Denotes Slip

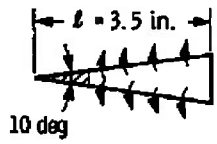

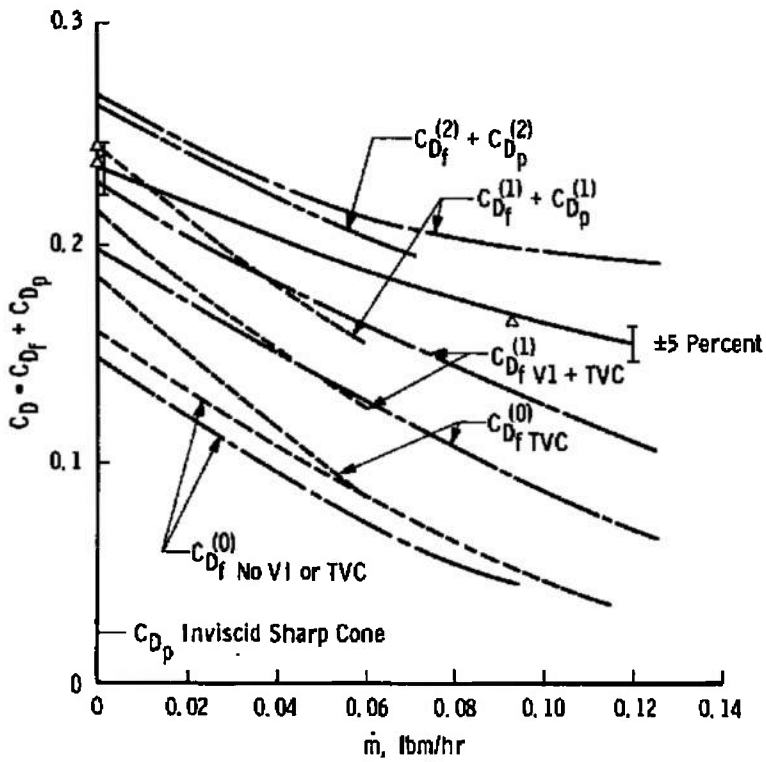

b. $M_\infty = 5.64$

Fig. 9 Concluded

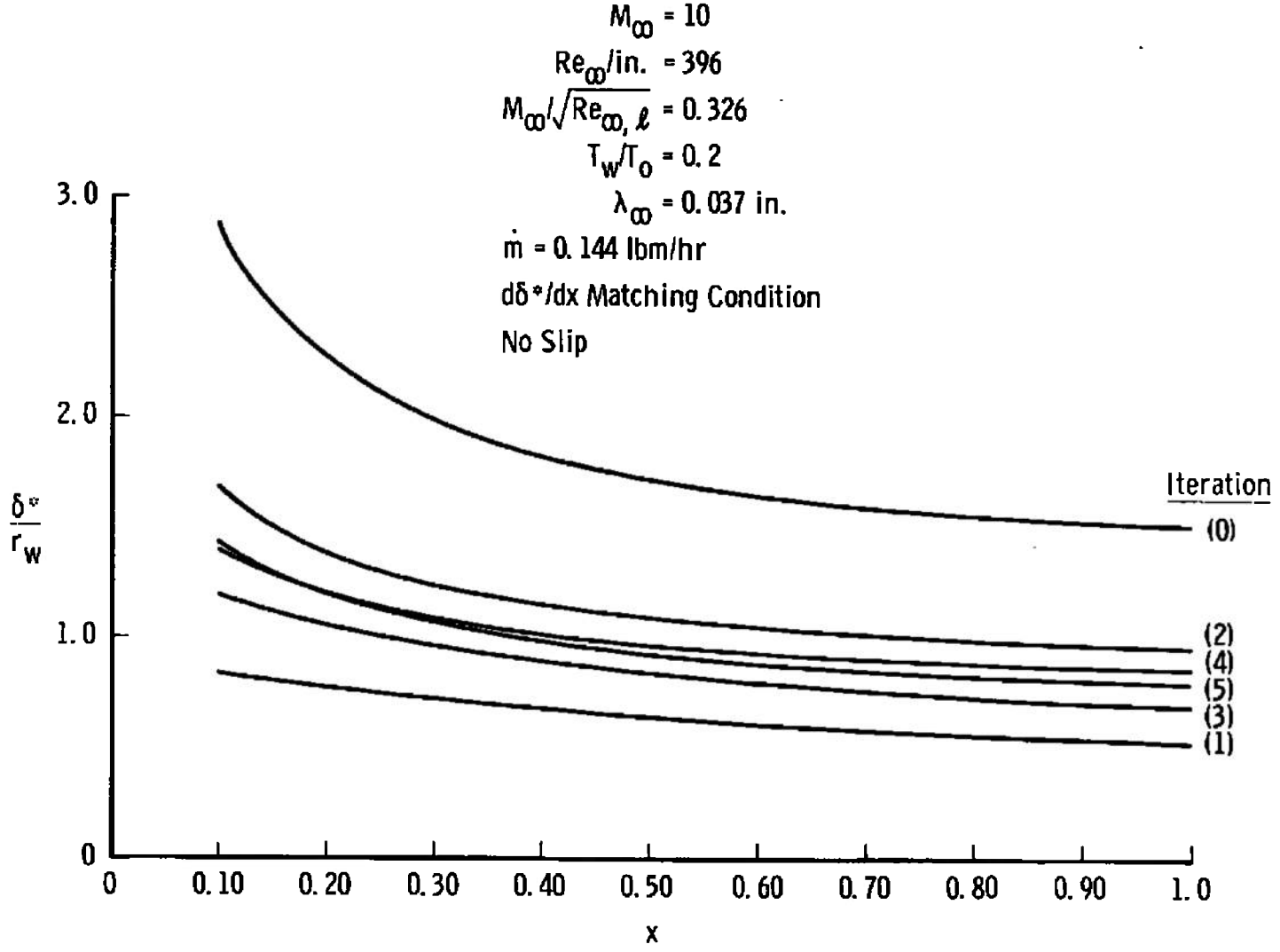

a. On Displacement Thickness

Fig. 10 Effects of Iteration with Mass Transfer

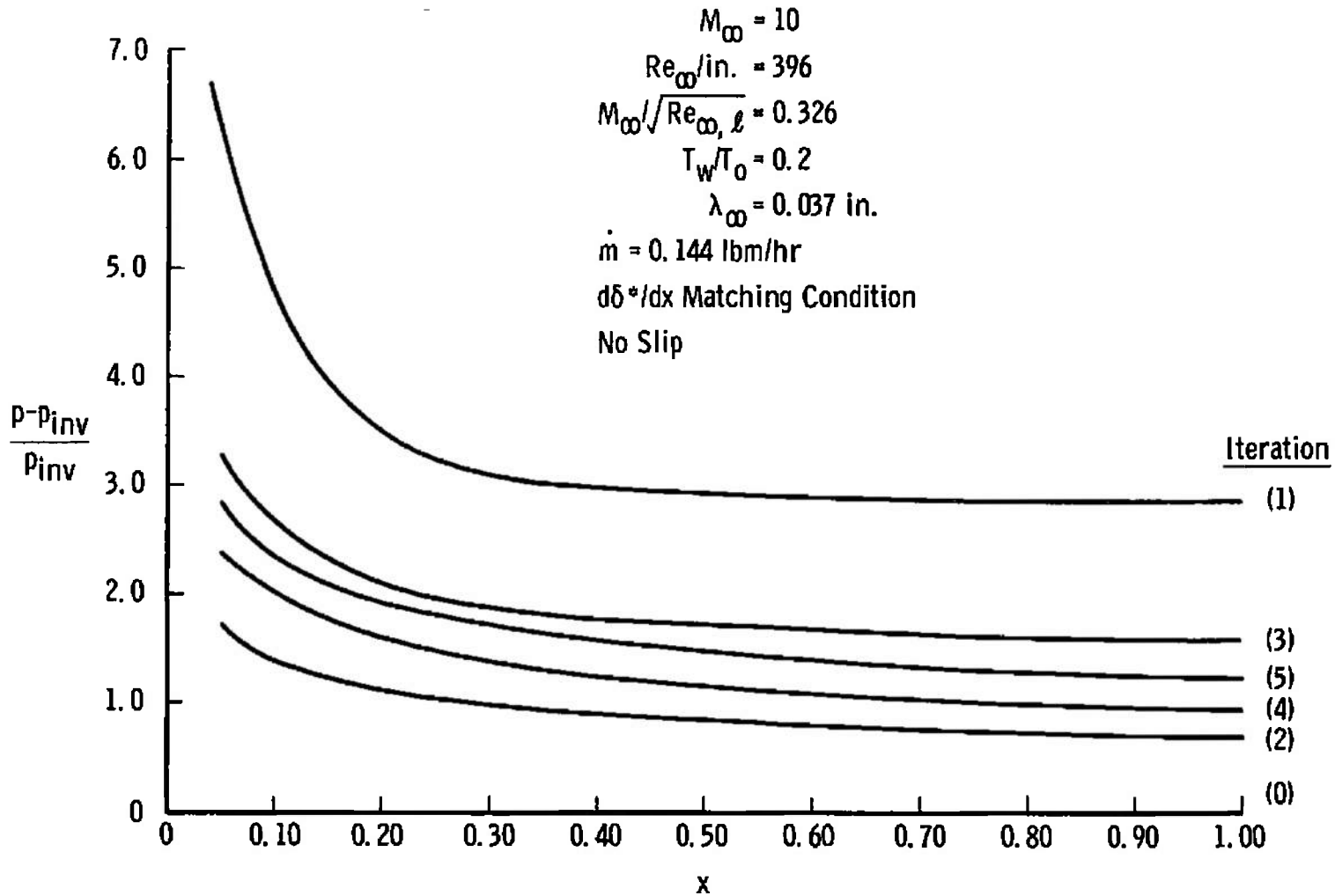

b. On Viscous-Induced Pressure

Fig. 10 Concluded

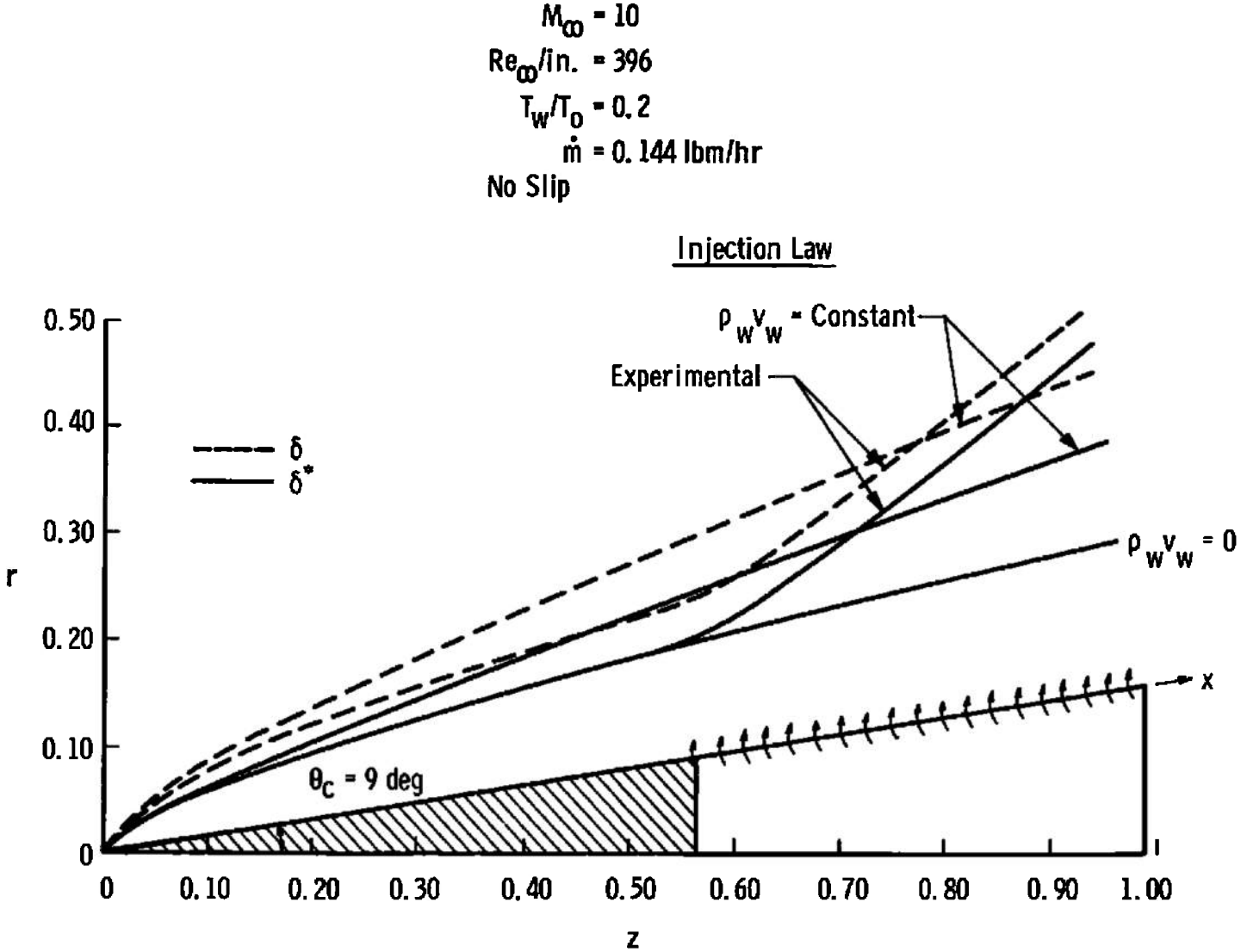

Fig. 11 Effects of Different Injection Laws on $\delta^{*(0)}$ with $\delta^{(0)}$ with Transverse Curvature

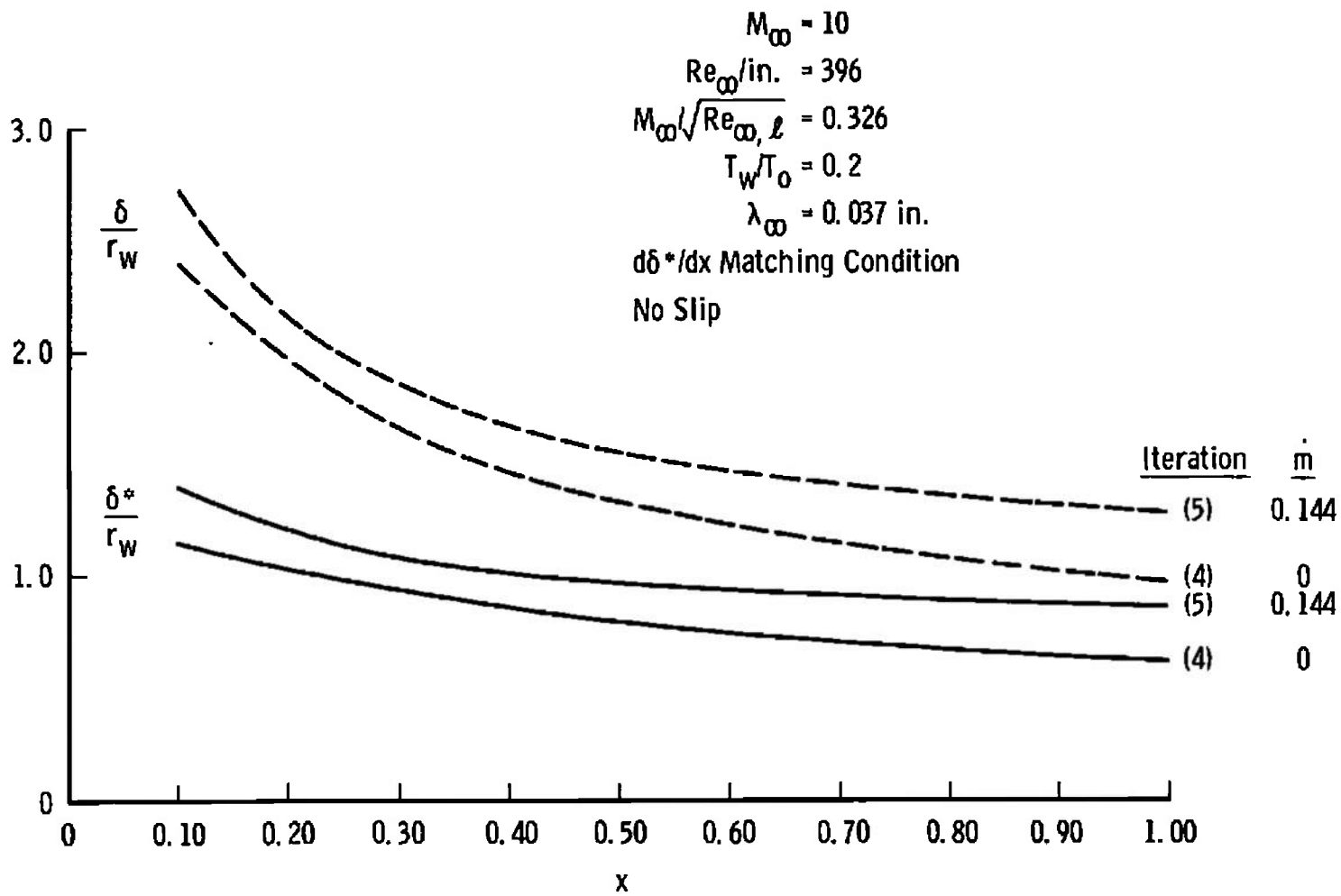

Fig. 12 Effects of Mass Transfer and Iteration on Displacement and Total Boundary-Layer Thicknesses

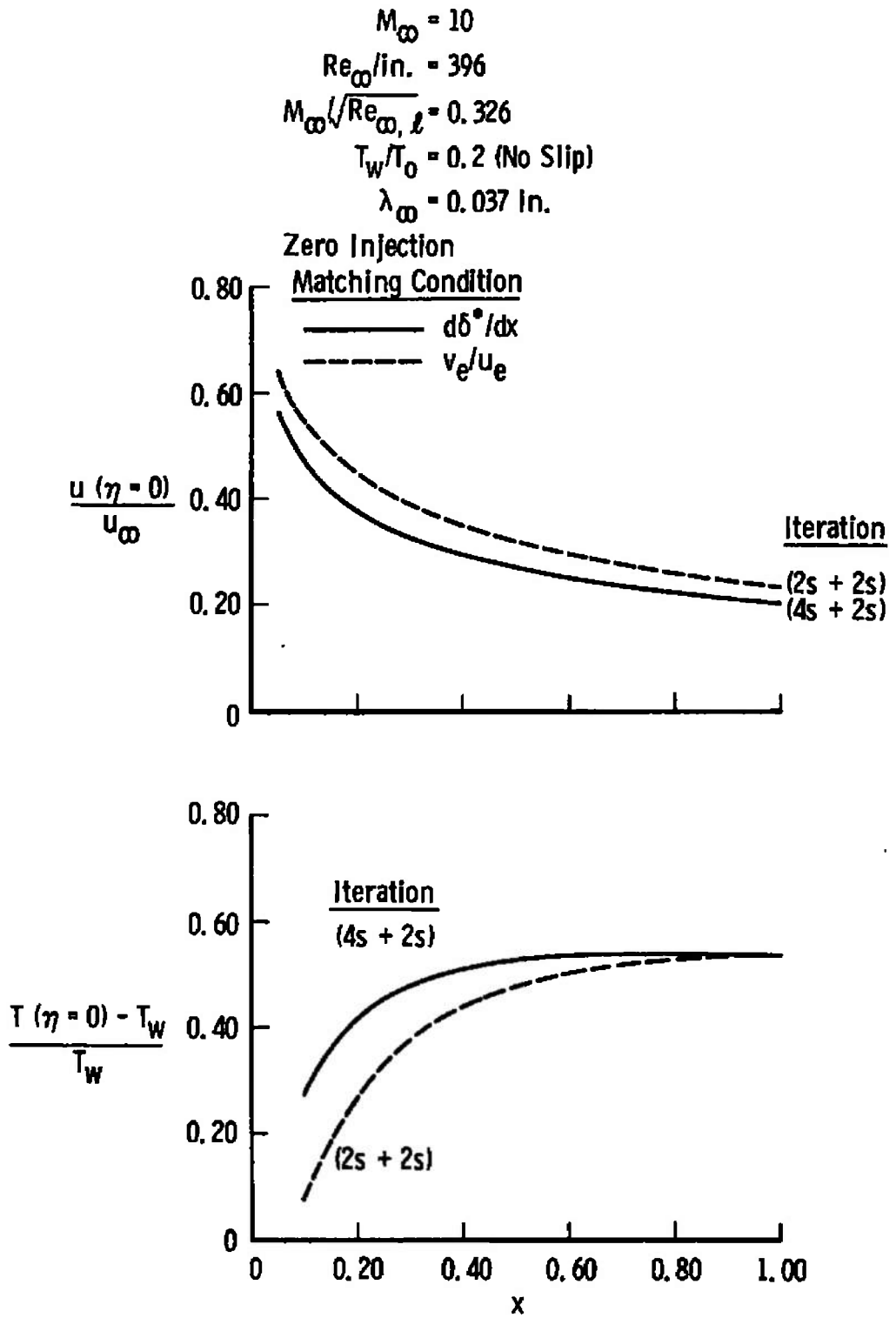

Fig. 13 Wall Slip and Temperature Jump under Rarefied Flow Conditions

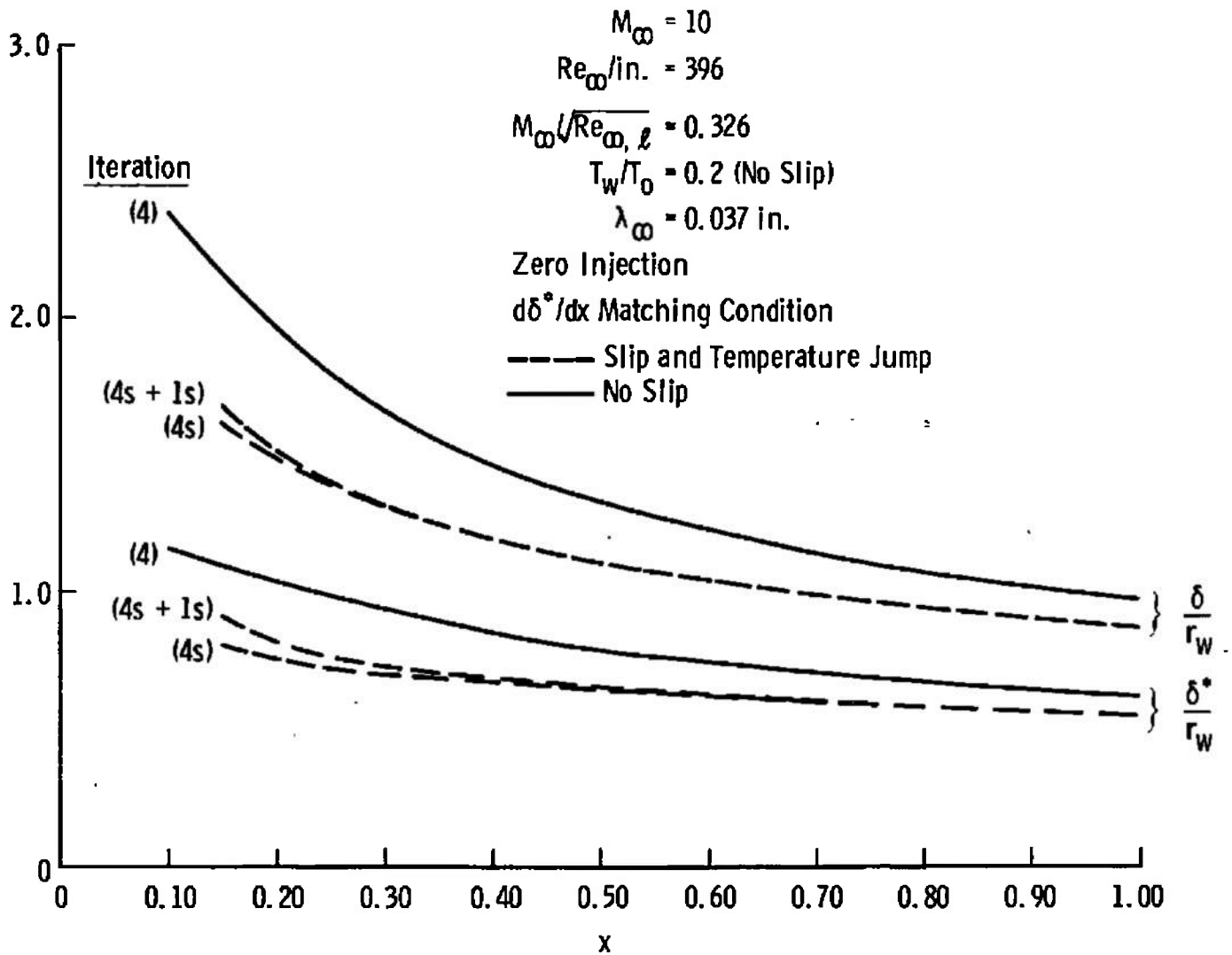

Fig. 14 Effects of Slip and Temperature Jump on Displacement and Total Boundary-Layer Thicknesses

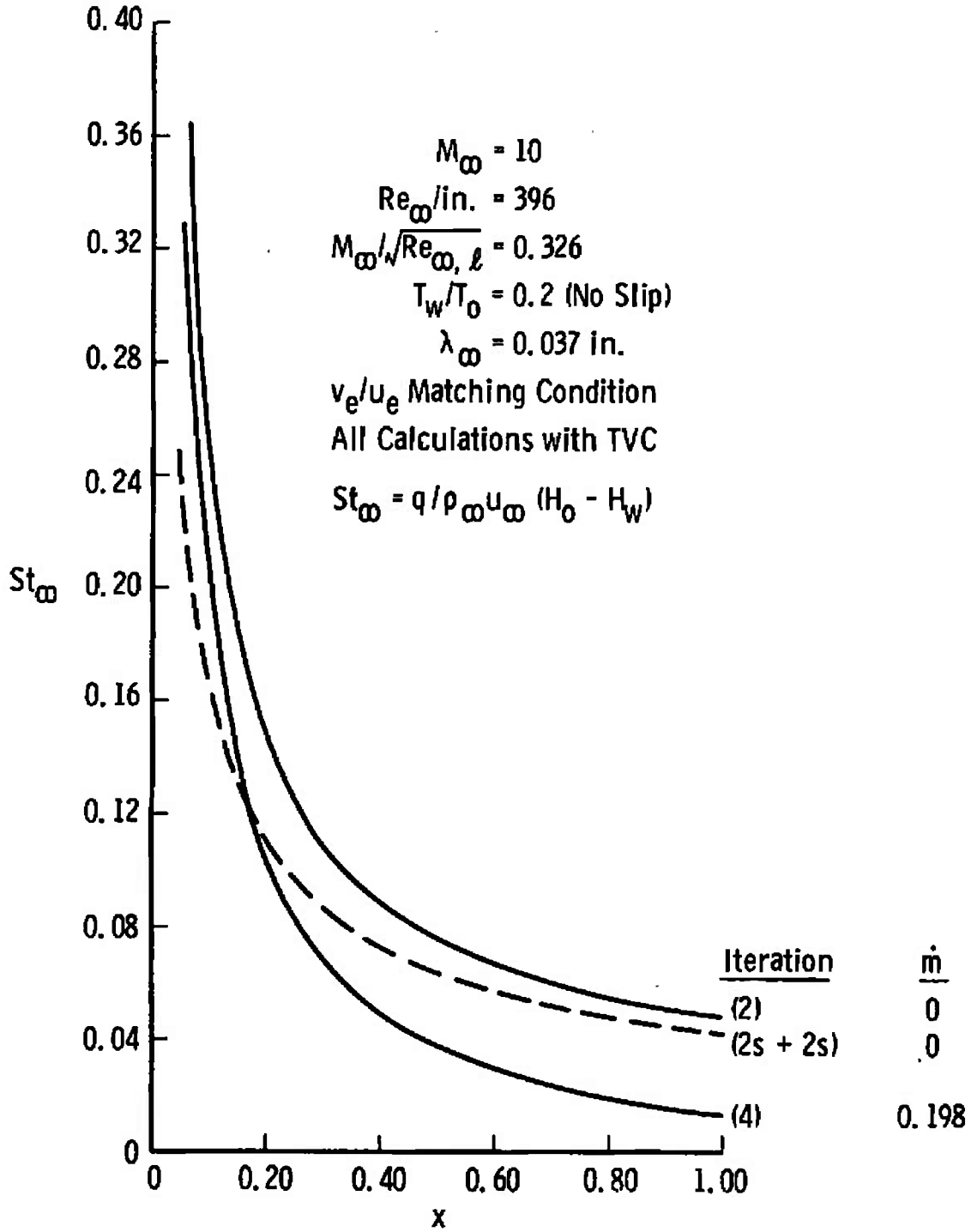

b. On Stanton Number

Fig. 16 Concluded

Experimental Data

Sym	M_∞	Re_∞/in.	T_0, °K	T_w, °K
□	9.38	2606	1033	~293
○	9.37	1602	1662	~293
△	10.15	388	3020	~293

Flagged Symbols Uncorrected Data

Numerical Results

Sym	M_∞	Re_∞/in.	T_0, °K	T_w/T_∞	T_w/T_0
—·—	9.37a	2869	1073	4.95	0.273
———	9.37b	1632	1835	2.76	0.160
— — —	10.0	396	3034	2.02	0.097

Note: All boundary-layer calculations include viscous interaction, transverse curvature, slip, and temperature jump.

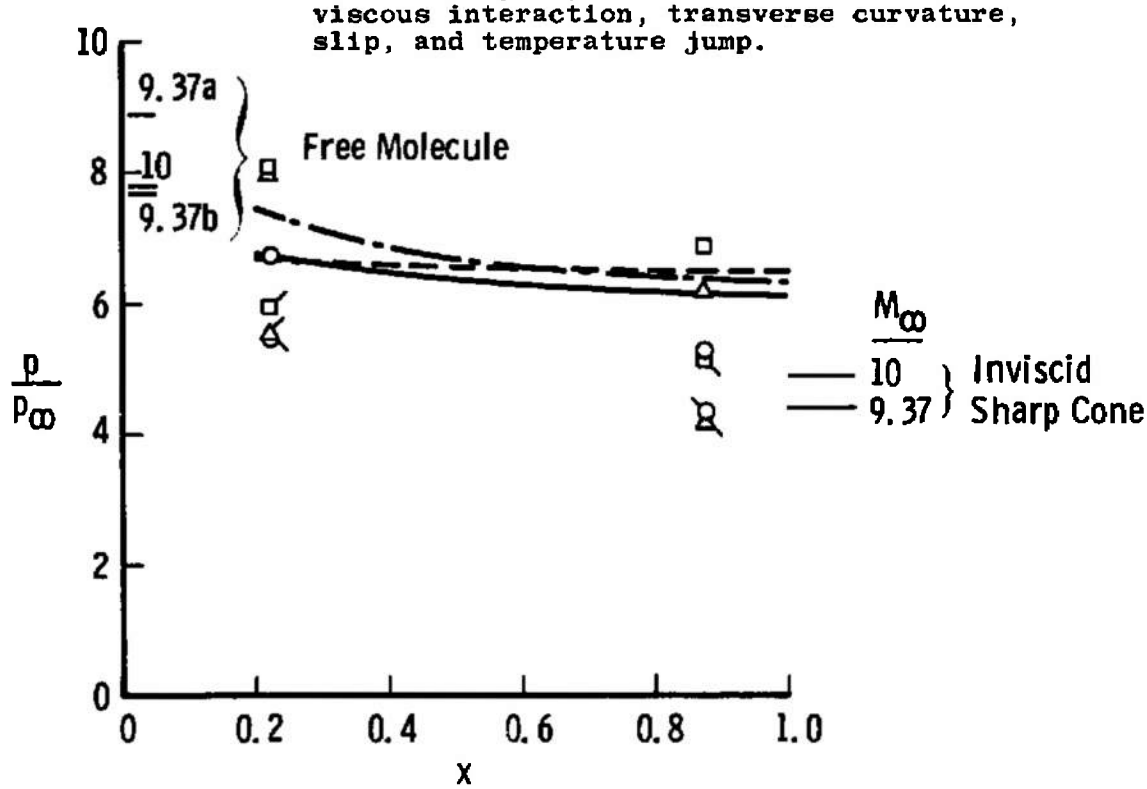

Fig. 17 Experimental and Theoretically Predicted Surface Pressures on a Water-Cooled 9-deg Half-Angle Cone at M_∞ = 10

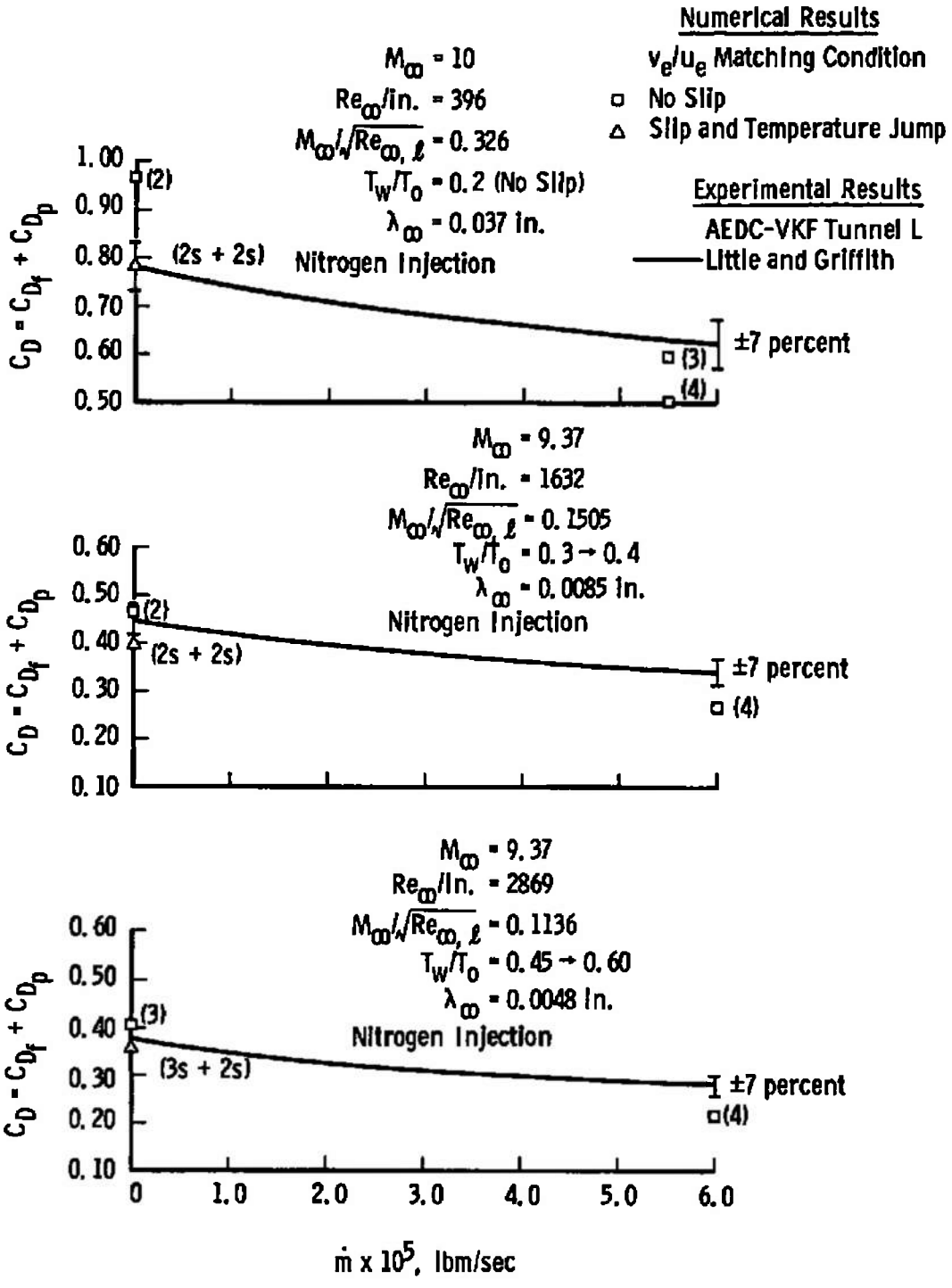

Fig. 18 Experimental and Theoretically Predicted Zero-Lift Drag with Mass Transfer

$M_\infty = 10$
$Re_\infty/in. = 22,528$
$M_\infty/\sqrt{Re_{\infty,\ell}} = 0.043$
$T_W/T_0 = 0.33 \rightarrow 0.75$
$\lambda_\infty = 0.00066$
Nitrogen Injection

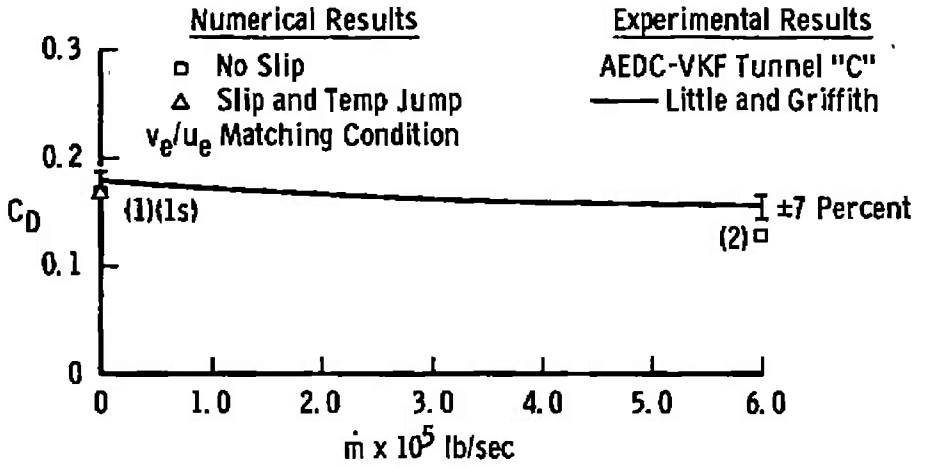

$M_\infty = 10$
$Re_\infty/in. = 45,057$
$M_\infty/\sqrt{Re_{\infty,\ell}} = 0.0306$
$T_W/T_0 = 0.33 \rightarrow 0.75$
$\lambda_\infty = 0.00033$ in.
Nitrogen Injection

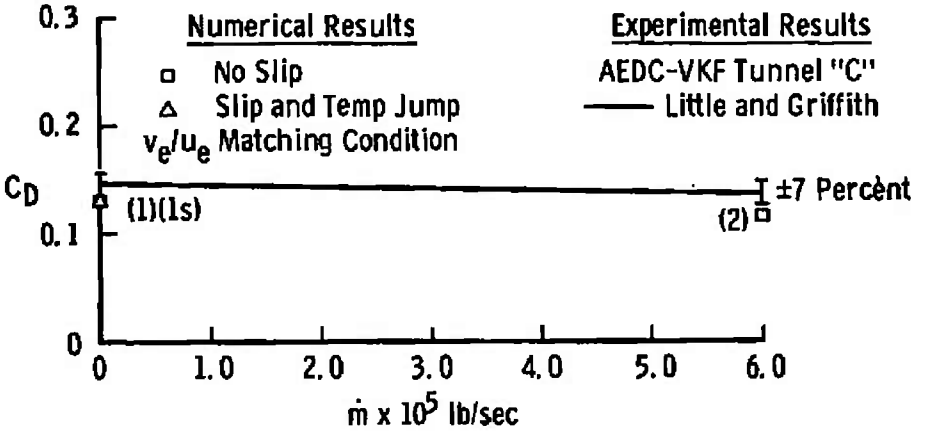

Fig. 18 Concluded

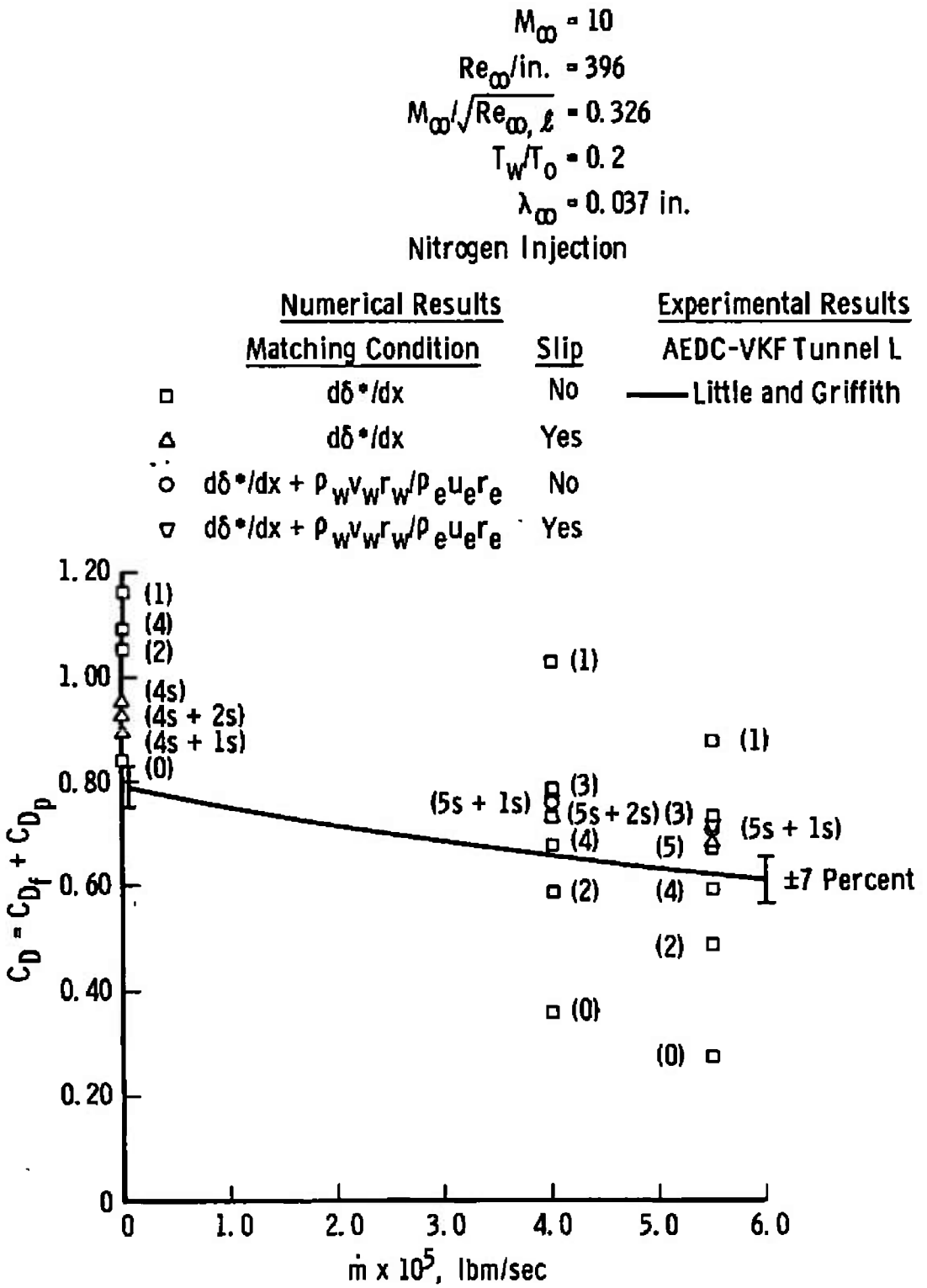

Fig. 19 Effects of Iteration, Mass Transfer, Slip, and Temperature Jump on Zero-Lift Drag at M_∞ = 10

Experimental Data

Sym	M_∞	Re_∞/in.	θ_c, deg	T_0, °K	T_w/T_0	C_∞	λ_∞, in.	Tunnel	Source
○	10.15	388	9	3,020	0.30	0.630	0.037	L	Little and Griffith
□	9.37	1,600	9	1,662	0.50	0.649	0.0085	L	
◁	9.38	2,600	9	1,033	~0.65	0.701	0.0048	L	
◇	10.00	23,800	9	958	~0.75	0.660	0.00066	C	
⬭	10.00	42,600	9	958	~0.75	0.685	0.00033	C	
△	3.93	1,765	5	300	0.96	0.821	0.0032	Berkeley	King and Talbot
◇	5.64	6,200	5	300	0.96	0.815	0.0012	Berkeley	King and Talbot
▨									Whitfield and Griffith (1963)

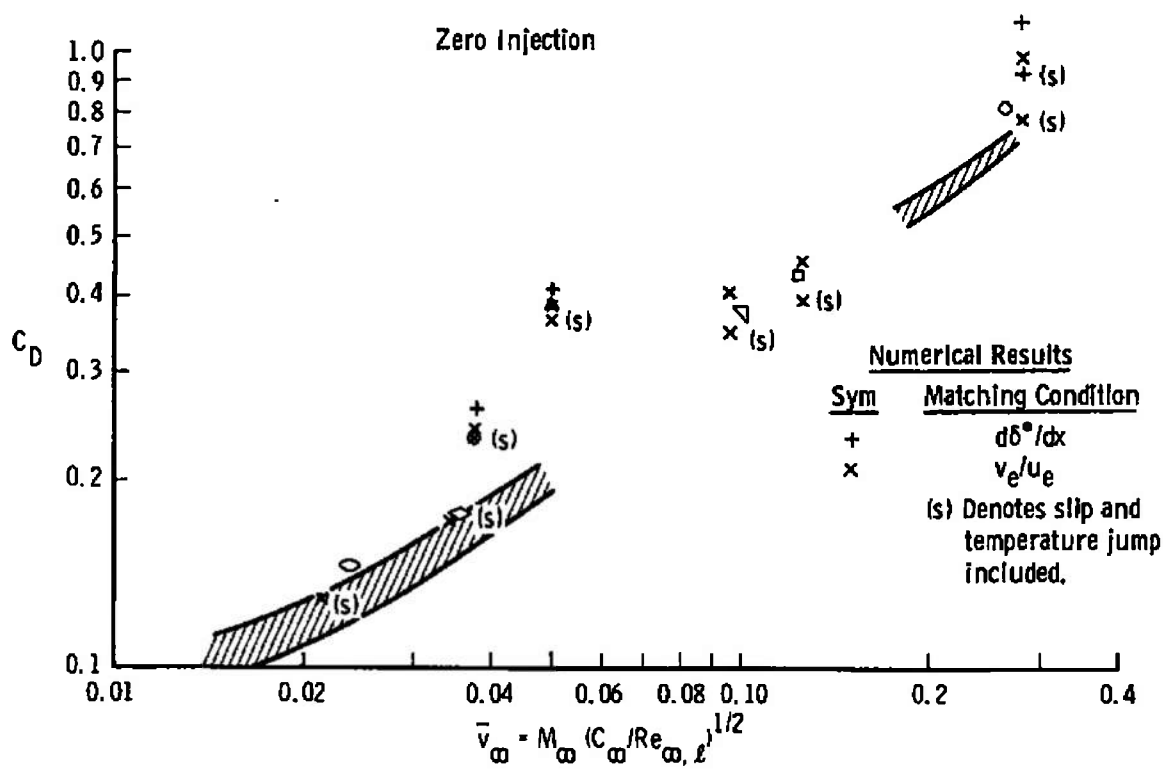

Fig. 20 Experimental and Theoretically Predicted Zero-Lift Drag of Sharp Slender Cones

TABLE I
CONDITIONS USED IN THE EXPERIMENTAL AND NUMERICAL STUDIES

Tunnel	M_∞	$Re_\infty/in.$	p_0', psia	$H_0 \times 10^{-7}$, ft^2/sec^2	p_0, psia	T_0, °K	$P_\infty \times 10^3$, psia	T_∞, °K	$\rho_\infty \times 10^6$, $lbf\text{-}sec^2/ft^4$	U_∞, ft/sec	C_∞
Berkeley Low Density Tunnel											
	3.93	1765	0.0334	0.3245	0.227	300	1.64	73.4	1.04	2215	0.821
	5.64	6200	0.0679	0.3245	1.775	300	1.64	40.7	1.875	2368	0.815
AEDC-VKF Hypersonic Tunnels[a]											
L[b]	10.15	388	0.0507	3.930	18.00	3020	0.397	144.5	0.124	8118	0.630
	(10.00)	(396)		(3.395)	(16.64)	(3034)	0.392		(0.122)	(8041)	0.728
L	9.37	1602	0.1056	2.053	25.00	1662	0.952	93.0	0.461	6030	0.649
		(1632)			(25.62)	(1835)	(0.930)	(98.9)	(0.429)	(6194)	0.678
L	9.38	2606	0.0812	1.200	19.50	1033	0.713	56.8	0.565	4778	0.701
	(9.37)	(2869)			(19.70)	(1073)	(0.715)	(57.8)	(0.552)	(4766)	0.710
C	10.00	42,640	0.978	1.076	350	958	7.85	45.6	8.01	4444	0.660
		(45,057)			(321.3)	(994)	(7.57)	(47.3)	(7.44)	(4526)	0.675
C	10.00	23,820	0.488	1.076	175	958	4.13	47.3	4.06	4444	0.685
		(22,528)			(160.4)	(994)	(3.78)		(3.72)	(4526)	0.675

[a]Unless otherwise noted ideal gas data computed from H_0, p_0', and M_∞ shown in parentheses.

[b]Ideal gas data computed from p_0', T_∞, and M_∞ shown in parentheses.

TABLE II
EXPERIMENTAL DATA ON THE EFFECTS OF MASS TRANSFER ON ZERO-LIFT DRAG

Tunnel	M_∞	Re_∞/in.	$\dot{m}$, lbm/hr	T_w/T_o	C_D
Berkeley Low Density Tunnel					
	3.93	1765	0	0.96	0.386
			0.03125		0.339
			0.0625		0.290
			0.09375		0.253
	5.64	6200	0	0.96	0.235
			0.03125		0.211
			0.0625		0.186
			0.09375		0.167
AEDC-VKF Hypersonic Tunnels[a]					
L	10.15	388	0	0.3	0.788
			0.0254	(0.1)	0.764
			0.1440	(0.1)	0.662
			0.1980	(0.1)	0.625
L	9.37	1602	0	0.5	0.443
			0.2160	(0.3)	0.340
L	9.38	2606	0	0.65	0.377
			0.2160	(0.45)	0.282
C	10.00	42,640	0	(0.75)	0.146
			0.2160	(0.33)	0.135
C	10.00	23,820	0	(0.75)	0.178
			0.2160	(0.33)	0.153

[a]Estimated equilibrium wall temperature ratios in parentheses.

TABLE III
EXPERIMENTAL WALL PRESSURE DATA ON A 9-DEG WATER-COOLED CONE IN TUNNEL L

M_∞	x	p_m/p_∞	p_c/p_∞[a]
9.38	0.222	5.98	8.11
	0.877	5.15	6.83
9.37	0.222	5.51	6.72
	0.877	4.30	5.23
10.15	0.222	5.58	8.00
	0.877	4.11	6.17

[a]Pressures corrected for orifice size after Potter, Kinslow, and Boylan (Ref. 13).

TABLE IV
EXPERIMENTAL EQUILIBRIUM WALL-TO-STAGNATION TEMPERATURE DATA ON A THIN-WALLED STAINLESS STEEL MODEL IN TUNNEL L

M_∞	9.38	9.37	10.15
T_o, °K	1033	1662	3020
x	T_w/T_o		
0.079	0.817	0.546	0.307
0.342	0.675	0.514	0.296
0.526	0.654	0.507	0.294
0.658	0.650	0.506	0.286

UNCLASSIFIED

Security Classification

DOCUMENT CONTROL DATA - R&D

(Security classification of title, body of abstract and indexing annotation must be entered when the overall report is classified)

1. ORIGINATING ACTIVITY (Corporate author)	2a. REPORT SECURITY CLASSIFICATION
Arnold Engineering Development Center ARO, Inc., Operating Contractor Arnold Air Force Station, Tennessee	UNCLASSIFIED
	2b GROUP N/A

3. REPORT TITLE

MASS TRANSFER AND FIRST-ORDER BOUNDARY-LAYER EFFECTS ON SHARP CONE DRAG

4. DESCRIPTIVE NOTES (Type of report and inclusive dates)

N/A

5. AUTHOR(S) (Last name, first name, initial)

Clark H. Lewis, Ernest O. Marchand, and Herbert R. Little, ARO, Inc.

6. REPORT DATE	7a. TOTAL NO. OF PAGES	7b. NO. OF REFS
March 1966	62	19

8a. CONTRACT OR GRANT NO.	9a. ORIGINATOR'S REPORT NUMBER(S)
AF40(600)-1200 b. PROJECT NO. 8953 c. Task 895303 d. Program Element 62405334	AEDC-TR-66-37
	9b OTHER REPORT NO(S) (Any other numbers that may be assigned this report) N/A

10. AVAILABILITY/LIMITATION NOTICES Qualified users may obtain copies of this report from DDC. Distribution of this document is unlimited.

11. SUPPLEMENTARY NOTES	12. SPONSORING MILITARY ACTIVITY
N/A	Hq, Arnold Engineering Development Center, Air Force Systems Command, Arnold Air Force Station, Tenn.

13. ABSTRACT A theoretical model is developed based on an iterated perfect gas inviscid-viscous flow field which includes first-order displacement (viscous interaction), transverse curvature, wall slip, and temperature jump in addition to mass transfer effects. The effects of inviscid (tangent cone) and viscous (nonsimilar laminar boundary layer) flow field matching conditions are also considered. Numerical results are compared with experimental and analytical results of King and Talbot (AIAA J., 1964) for a 5-deg half-angle cone at M_∞ = 3.93 and 5.64. The predicted viscous-induced pressure without mass transfer and the zero-lift drag with and without injection were in agreement with the experimental data within experimental uncertainty. The theoretical model was also used to predict zero-lift drag of a 9-deg half-angle cone at M_∞ = 9.37 and 10 and Re_∞/in. = 400 to 45,000 for a range of wall-to-stagnation temperature ratios. Again, in general, without mass transfer the predictions were within experimental uncertainty. The inability of the theoretical model to adequately treat nonuniform mass transfer distributions is discussed. At the lowest Reynolds number the effects of slip were most significant. At all conditions the effects of inviscid-viscous flow field matching were significant. Experimental zero injection equilibrium wall temperature distributions and cool-wall pressure data are given at M_∞ ~ 10 and Re_∞/in. = 400 to 2600.

DD FORM 1 JAN 64 1473

UNCLASSIFIED

Security Classification

14. KEY WORDS	LINK A		LINK B		LINK C	
	ROLE	WT	ROLE	WT	ROLE	WT
mass transfer						
boundary layer effects						
conical bodies						
drag						
hypersonic flow						
theoretical models						
viscous interaction						
transverse curvature						
wall slip						
temperature jump						

INSTRUCTIONS

1. ORIGINATING ACTIVITY: Enter the name and address of the contractor, subcontractor, grantee, Department of Defense activity or other organization *(corporate author)* issuing the report.

2a. REPORT SECURITY CLASSIFICATION: Enter the overall security classification of the report. Indicate whether "Restricted Data" is included. Marking is to be in accordance with appropriate security regulations.

2b. GROUP: Automatic downgrading is specified in DoD Directive 5200.10 and Armed Forces Industrial Manual. Enter the group number. Also, when applicable, show that optional markings have been used for Group 3 and Group 4 as authorized.

3. REPORT TITLE: Enter the complete report title in all capital letters. Titles in all cases should be unclassified. If a meaningful title cannot be selected without classification, show title classification in all capitals in parenthesis immediately following the title.

4. DESCRIPTIVE NOTES: If appropriate, enter the type of report, e.g., interim, progress, summary, annual, or final. Give the inclusive dates when a specific reporting period is covered.

5. AUTHOR(S): Enter the name(s) of author(s) as shown on or in the report. Enter last name, first name, middle initial. If military, show rank and branch of service. The name of the principal author is an absolute minimum requirement.

6. REPORT DATE: Enter the date of the report as day, month, year, or month, year. If more than one date appears on the report, use date of publication.

7a. TOTAL NUMBER OF PAGES: The total page count should follow normal pagination procedures, i.e., enter the number of pages containing information.

7b. NUMBER OF REFERENCES: Enter the total number of references cited in the report.

8a. CONTRACT OR GRANT NUMBER: If appropriate, enter the applicable number of the contract or grant under which the report was written.

8b, 8c, & 8d. PROJECT NUMBER: Enter the appropriate military department identification, such as project number, subproject number, system numbers, task number, etc.

9a. ORIGINATOR'S REPORT NUMBER(S): Enter the official report number by which the document will be identified and controlled by the originating activity. This number must be unique to this report.

9b. OTHER REPORT NUMBER(S): If the report has been assigned any other report numbers *(either by the originator or by the sponsor)*, also enter this number(s).

10. AVAILABILITY/LIMITATION NOTICES: Enter any limitations on further dissemination of the report, other than those imposed by security classification, using standard statements such as:

(1) "Qualified requesters may obtain copies of this report from DDC."

(2) "Foreign announcement and dissemination of this report by DDC is not authorized."

(3) "U. S. Government agencies may obtain copies of this report directly from DDC. Other qualified DDC users shall request through _____."

(4) "U. S. military agencies may obtain copies of this report directly from DDC. Other qualified users shall request through _____."

(5) "All distribution of this report is controlled. Qualified DDC users shall request through _____."

If the report has been furnished to the Office of Technical Services, Department of Commerce, for sale to the public, indicate this fact and enter the price, if known.

11. SUPPLEMENTARY NOTES: Use for additional explanatory notes.

12. SPONSORING MILITARY ACTIVITY: Enter the name of the departmental project office or laboratory sponsoring *(paying for)* the research and development. Include address.

13. ABSTRACT: Enter an abstract giving a brief and factual summary of the document indicative of the report, even though it may also appear elsewhere in the body of the technical report. If additional space is required, a continuation sheet shall be attached.

It is highly desirable that the abstract of classified reports be unclassified. Each paragraph of the abstract shall end with an indication of the military security classification of the information in the paragraph, represented as *(TS)*, *(S)*, *(C)*, or *(U)*

There is no limitation on the length of the abstract. However, the suggested length is from 150 to 225 words.

14. KEY WORDS: Key words are technically meaningful terms or short phrases that characterize a report and may be used as index entries for cataloging the report. Key words must be selected so that no security classification is required. Identifiers, such as equipment model designation, trade name, military project code name, geographic location, may be used as key words but will be followed by an indication of technical context. The assignment of links, rules, and weights is optional.